3D geometrical modelling of the non-cylindrical Vélodrome Miocene fold in the southwestern Alps

Agathe Faure, Nicolas Loget, Laurent Jolivet, Charles Gumiaux, Cécile Allanic, Jean-Paul Callot, Gautier Laurent, Nicolas Bellahsen, Myette Guiomar

Journal Pre-proof

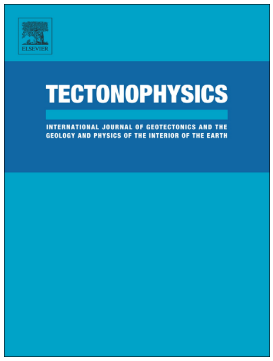

3D geometrical modelling of the non-cylindrical Vélodrome Miocene fold in the southwestern Alps

Agathe Faure, Nicolas Loget, Laurent Jolivet, Charles Gumiaux, Cécile Allanic, Jean-Paul Callot, Gautier Laurent, N. Bellahsen, Myette Guiomar

PII: S0040-1951(24)00098-2

DOI: https://doi.org/10.1016/j.tecto.2024.230296

Reference: TECTO 230296

To appear in: *Tectonophysics*

Received date: 11 December 2023

Revised date: 23 March 2024

Accepted date: 24 March 2024

Please cite this article as: A. Faure, N. Loget, L. Jolivet, et al., 3D geometrical modelling of the non-cylindrical Vélodrome Miocene fold in the southwestern Alps, *Tectonophysics* (2023), https://doi.org/10.1016/j.tecto.2024.230296

3D geometrical modelling of the non-cylindrical Vélodrome Miocene fold in the southwestern Alps

Agathe Faure[1], Nicolas Loget[1], Laurent Jolivet[1], Charles Gumiaux[2], Cécile Allanic[3], Jean-Paul Callot[4], Gautier Laurent[2], N. Bellahsen[1], Myette Guiomar[5]

[1]Sorbonne Université, CNRS-INSU, Institut des Sciences de la Terre de Paris (ISTeP), UMR 7193 – France

[2]Univ. Orléans, CNRS, BRGM, ISTO, UMR 7327, F-45071, Orléans, France

[3]Bureau de Recherches Géologiques et Minières (BRGM) - France

[4]E2S UPPA CNRS/TOTAL/Univ Pau & Pays Adour, Laboratoire Des Fluides Complexes Et Leurs Reservoirs-IPRA, UMR5150 - France

[5]Réserve Naturelle Nationale Géologique de Haute Provence (RNNGHP) France

Abstract :

Fold geometries and kinematics within foreland basins is a major issue for understanding the late evolution of thrust fronts. In the foreland of the southwestern Alps, the Vélodrome complex fold involves the whole Tertiary series which have recorded the evolution of the alpine front. From a geometrical and kinematic point of view, the Vélodrome is classically described as a recumbent Mio-Pliocene syncline with a strongly curved axis; interpreted either as a classic growth-fold, a post-deposit fold, or a result of coeval salt activity. The debate reveals a lack of consensus on the internal structure of the Vélodrome and the potential role of salt motion. By a detailed field analysis coupled with an implicit 3D geometrical modelling approach, we test the different hypotheses and provide a new 3D illustrated interpretation of the Vélodrome series. The Vélodrome consists in a complex non-cylindrical structure composed by several folds with different orientations together with inter- and intra-formations unconformities. Folding is partly syn-depositional and began earlier in the south, near Esclangon village, than in the north. In the north, deformation started with the marly and sandy molasse (m2, middle Burdigalian), attested by the transition from the conformable conglomeratic marine molasse (m1-2, Aquitanian and early Burdigalian) to the unconformable m2 to the Valensole formation. Deformation began earlier in the south, during the deposition of the m1-2, as shown by internal unconformities. We discuss the ingredients controlling the deformation in the Vélodrome, regional tectonics (mainly since middle Burdigalian) versus salt tectonics. This study further brings new constraints on the timing and pattern of deformation of the southwestern orogenic front of the Alps. It also highlights the power of the 3D geometrical modelling approach for testing different hypotheses and better understanding 3D complex structures.

Keywords:

Digne Nappe, Southwestern Alps, 3D geometrical modelling, Vélodrome

1. Introduction

The external parts of mountain belts, including their foreland basins, classically present a fold-and-thrust belt often detached on shallow decollement levels. In order to decipher both the deformation sequence and the deformation pattern, the study of fold kinematics coupled with syntectonic depocenters related to growth structures is crucial (Leeder, 2011; DeCelles, 2012). The west Alpine foreland thrust belt shows many such structures constraining the Oligo-

Miocene evolution of the Alpine deformation front (Beck et al., 1998; Lickorish and Ford, 1998, Fournier et al., 2008, Kalifi et al., 2021). This paper is focused on the well-known "Vélodrome fold" included in the Digne basin, at the front of the sub-Alpine Digne Nappe (Fig.1). Classically, the trend of foreland fold axes can be used as a regional proxy of the perpendicular to the maximum shortening direction (e.g., Nabavi and Fossen, 2021). However, the Vélodrome belongs to a second group of folds with axes oblique to the principal shortening direction or non-cylindrical folds. They result from various causes such as structural inheritance, salt-related mechanisms or polyphase episodes, making the classical approach challenging (e.g. Callot et al., 2012) and blurring our understanding of the propagation of the sub-Alpine domain front.

Pre-folding tectonic features (basement lows and highs, earlier faults or folds, contrast in thicknesses and mechanical architecture of the sedimentary pile) may influence fold geometry, the orientation of structures with respect to the main regional shortening direction, the partitioning of strain or the overall style of folds (Ahmadhadi et al., 2008; Tavani et al., 2015; Rodrigues et al., 2021). Fold interference studies show that non-cylindrical folds can also be associated with the succession of deformation events (Ramsay, 1962; Marroni et al., 2002) or interfering coevals events with different kinematics (Ghosh et al., 1996; Balestra et al., 2019). Salt dynamic can also influence the geometry and the kinematics of fold-and-thrust belts at various scales (Davis and Engelder, 1985; Scrocca, 2006; Callot et al., 2012; Duffy et al., 2018; Granado et al., 2019; Legeay et al., 2019; Jourdon et al., 2020, Burrel and Teixell, 2021). Salt influence results either from salt activity during the genesis and development of the orogenic wedge, or from the inheritance of pre-existing salt-related structures, such as diapirs triggered by extension during the rifting phase (Jackson and Vendeville, 1994; Callot et al., 2007; Callot et al., 2012; Decarlis et al., 2014; Granado et al., 2019; Célini et al., 2020a). In the sub-Alpine domain, recent studies have highlighted the role of salt activity during the whole evolution of the Alpine realm, from the passive margin development to its involvement into the Alpine belt (Graham et al., 2012; Decarlis et al., 2014; Célini et al., 2020a, 2021, 2022; Brooke-Barnett, 2022), providing notable new insights on the genesis of complex folds in the Digne Nappe (Célini et al., 2020a, 2021).

The Vélodrome is a complex fold in the foreland of the western Alps serving as a field school for many French and European universities. The outcropping conditions and the variety of sedimentary facies and tectonic structures make it ideal for learning geological mapping and understanding structures in 3-D. This region has thus been intensely explored by generations of geologists and students. Yet, despite excellent geological maps and numerous cross-sections published, some first-order scientific questions remain non-consensual about the 3D geometry

of the Velodrome and its mechanism of formation. From a geometrical and kinematic point of view, the Vélodrome is classically described as a recumbent Mio-Pliocene syncline with a strongly curved axis (Gidon and Pairis, 1992). This complex fold is the main place where Tertiary deposits crop out continuously (from the Oligocene to the late Mio-Pliocene), thus offering a perfect laboratory for studying foreland basin deformation and late orogenic front evolution, either as (1) a classic growth-fold (Gigot et al., 1974; Crumeyrolle et al., 1991), (2) a post-sedimentation fold (Fournier et al., 2008) or (3) a result of coeval salt activity in this area (Célini et al., 2022). (1) The Vélodrome has often been interpreted as a growth-fold evolving during the Miocene and Pliocene (Gigot et al., 1974; Gidon and Pairis, 1988, 1992; Haccard et al., 1989a) with internal unconformities recording the late shortening of the southwest Alps (ending with the Digne Nappe). (2) Fournier et al. (2008) challenged this interpretation and favoured a post-sedimentation folding, forming in the late Miocene and Pliocene age (contemporaneous of the Digne Nappe emplacement), based on microstructural analyses. (3) Recently, the reassessment of the Miocene Vélodrome geometries (unconformities and thickness variations) in the light of well-imaged salt-controlled structures from the Gulf of Mexico and Turkey allowed Graham et al. (2012) and Célini et al. (2022) to compare its geometry with known salt-related mini-basins (Giles and Rowan, 2012; Callot et al., 2014, 2016; Ribes et al., 2015; Kergaravat et al., 2016, 2017; Célini, 2020b) and to interpret the Vélodrome as a salt-controlled mini-basin emplaced on a thrust-fed salt body at the thrust front.

These three different interpretations have 3-D geometrical requirements such as the presence or absence of internal syn-tectonic unconformities with different geometries; testing these interpretations thus requires that the 3-D geometry is more precisely constrained. Computing the 3-D structure with numerical approaches is a powerful mean of proposing different geometrical solutions, fully consistent in 3-D, and test them by comparison with field observations in cross-sections and maps, which is the goal of the present paper.

Constraining the 3-D structure of non-cylindrical structures such as the Vélodrome fold is a complex endeavor as no simple rules can be used to infer the sub-surface geometry. Until now, most of works have used series of cross-sections in different directions as well as 3-D diagrams drawn by hand, but large uncertainties on the geometrical compatibility of these cross-sections in 3-D remain, hampering our ability to approach the kinematics of building these structures, especially in a region where numerous teams have worked since many years and each have their own views on the 3-D structure. In order to better characterize such non-cylindrical folds, 3D geometrical modelling has proven a valuable approach to decipher polyphased deformation

history (Bistacchi et al., 2008; Laurent et al., 2016; Zulauf et al., 2017; Burrel and Teixell, 2021).

The purpose of this paper is thus to test the different geometries of the Vélodrome proposed in the literature with such a numerical approach thanks to the implicit 3D modelling software package, Geomodeller (© BRGM-Intrepid Geophysics), and propose a quantitatively tested new geometry of the fold in 3-D and finally discuss the respective roles of (i) growth or passive folding, (ii) tectonic inheritance, (iii) salt-related mechanisms and (iv) polyphased deformation in the genesis of the Vélodrome fold. Our study provides a methodology to test complex non-cylindrical 3D geometries in foreland-and-thrust belts.

2. Geological setting

2.1. Southwestern sub-Alpine chain

The Southwestern sub-Alpine fold-and-thrust belt results from the inversion of the European passive margin of the Alpine Tethyan ocean and records the whole history of the Alpine orogenic cycle (Lemoine et al., 1986; Graciansky et al., 1988, 1989; Coward and Dietrich, 1989; Pfiffner, 2014). The rifting phase started during the Early Jurassic (middle Liassic), evolving till the Middle Jurassic (Lemoine et al., 1986; Dumont, 1988; Coward and Dietrich, 1989). It was marked by the synrift deposition of carbonates on top of the Upper Triassic evaporites (Haccard et al., 1989a) (Fig.2a). In addition to extension, salt tectonics was recorded as early as this rifting phase, as evidenced by diapirs, megaflaps, and halokinetic sequences emplaced since the Early Jurassic (Liassic) (Ehtechamzadeh Afchar and Gidon, 1974; Mascle et al., 1988; Dardeau et al., 1990; Dardeau and Graciansky, 1990; Graham et al., 2012; Decarlis et al., 2014; Célini et al., 2020a,b; Célini et al., 2021). Deep marine deposits, known as the ‘Terres Noires’ (late Bathonian to early Oxfordian), attest for an increase of subsidence, marking the Tethys opening and the beginning of the post-rift phase in the Middle Jurassic, which lasted until the late Early Cretaceous (Tricart, 1984; Lemoine et al., 1986; Coward and Dietrich, 1989; Haccard et al., 1989a). The Upper Jurassic and Lower Cretaceous platform deposits have recorded regional instabilities and synsedimentary re-working (e.g. slumps) (Haccard et al., 1989a). During lower to the middle of the Cretaceous, the southwestern domain of the alps also recorded the extensional and thermal pulse related to the Valaisan ocean inception (Célini et al., 2023).

From the Late Cretaceous to the late Eocene, the Southwestern sub-Alpine area has undergone the so-called Pyreneo-Provençal phase in the Provence region (Lemoine, 1972, 1986; Siddans, 1979; Graciansky et al., 1989; Lacombe and Jolivet, 2005; Andreani et al., 2010; Bestani et al., 2015). Then, during the late Eocene, the Alpine collision phase initiated in the hinterland (Coward and Dietrich, 1989; Pfiffner, 2014; Ford et al., 2006), inducing early foreland basin subsidence and gentle folding (Lickorish and Ford, 1998; Ford et al., 1999; Ford and Lickorish, 2004). From the end of Rupelian, shortening in the external zones increased and the foreland basin recorded the transition from flysch to molasse. This was associated by a more westward thrusting recorded for instance by the Embrunais-Ubaye Nappes (Kerckhove, 1969; Lickorish and Ford, 1998; Dumont et al., 2012). This major kinematic change is considered as the beginning of the true collision (Bellahsen et al., 2014), possibly related to a change in subduction dynamics (Vignaroli et al., 2009; Dumont et al., 2012). The sedimentation was dominated by continental deposits (e.g., fluvial red-clay of the 'Molasse Rouge') that migrated progressively westward and was progressively confined to small piggy-back basins (Haccard et al., 1989b; Lickorish and Ford, 1998; Ford et al., 1999, 2006; Ford and Lickorish, 2004; Apps et al., 2004; Kalifi et al., 2021). The end of the Oligocene was characterized by the transition to a lacustrine environment, followed by shallow marine sedimentation throughout the Early Miocene due to renewed flexuration (Haccard et al., 1989a; Ford et al., 1999; Ford and Lickorish, 2004). The infill of the Miocene foreland basin of south-eastern France corresponds to a transgression-regression megacycle starting in the Burdigalian and modulated by global sea-level variations inducing punctuated transgression and incision stages (Besson et al., 2005; Crumeyrolle et al., 1991).

From the Miocene to the Pliocene, the sub-Alpine area underwent a shift in structural style, from thin-skinned to thick-skinned, represented by a deepening of the decollement interface and the associated thrusting and exhumation of the external crystalline massifs (i.e. Pelvoux, Argentera) (Lickorish and Ford, 1998; Bellahsen et al., 2014; Schwartz et al., 2017, Kalifi et al., 2021, 2022). The foreland sedimentation evolves from upper Oligocene and Lower Miocene conglomerates and red beds (Chattian to Early Miocene) to Middle Miocene shallow marine deposits during Burdigalian and Langhian.

The Digne Nappe and its associated subsidiary thrust sheets (namely La Robine and Authon-Valavoire), the foremost thrust sheets of the area, moved around 20 km southwestward over the Triassic evaporitic decollement during late Alpine convergence (from late Eocene to Mio-Pliocene; Goguel, 1963; Gidon and Pairis, 1986; Lickorish and Ford, 1998; Graham et al.,

2012). The last deformation phase is associated with the late uplift and exhumation stage of the Argentera massif around 6Ma (Bigot-Cormier et al., 2000) responsible for the (re)activation of the Digne Nappe thrust by a transfer of deformation from the basement to the Triassic detachment (Bellahsen et al., 2014; Schwartz et al., 2017). This allows the overthrusting of the Late Miocene-Pliocene Valensole basin deposits by the Digne Nappe (Goguel, 1963; Gidon and Pairis, 1986; Lickorish and Ford, 1998; Ford and Lickorish, 2004). The sedimentation in the Valensole basin was dominated by fluvial conglomerates (Haccard et al., 1989a; Ford et al., 1999). The ultimate movements of the Digne Nappe and related thrust sheets are attributed to the Pleistocene (Jorda et al., 1992) and even to the late Quaternary (Hippolyte and Dumont, 2000; Hippolyte et al., 2011). These movements are attested by compressive deformation evidence recorded by the Quaternary sediments, such as uplifted, tilted, and overthrusted paleocanyons of the Bès and Bléone rivers (Hippolyte et al., 2011).

2.2. Digne Nappe and Barles half window area

The Digne Nappe thrust represents the outermost thrust of the orogenic front of the Southwestern sub-Alpine chain (Goguel, 1963; Gidon and Pairis, 1986; Lickorish and Ford, 1998; Ford and Lickorish, 2004). It extends over 100 km from west of the Pelvoux basement massif in the North, to the Barrême village in the South, connecting to the Castellane arc (Fig.1a) (Gidon and Pairis, 1986). The Digne Nappe uses the Triassic evaporite level as a decollement surface (Fig.2a) , as evidenced by the almost systematic presence of gypsiferous outcrops along its front, and at the sole of the thrust, also associated with diapiric structures (e.g. Pharaon unit, ‘complexe chaotique de Barles’) (Haccard et al., 1989a; Gidon, 1997; Célini et al., 2020b). The transport direction swings from WNW next to the Pelvoux basement massif, to WSW near Gap and south of Digne, to SSW around the Barles half-window, these changes in direction resulting both from a radial disposition during thrusting and timewise evolution of the shortening direction (Platt, 1986 and reference therein; Lickorish and Ford, 1998; Ford et al., 2006; Hippolyte et al., 2011; Dumont et al., 2012; Graham et al., 2012). The Upper Miocene to Pliocene conglomerates of the Valensole basin form the youngest deposits overlain by the Digne Nappe, as clearly seen south of Saint Geniez (Fig.1). The last increments of the Nappe displacement are coeval with the deposition of the syn-orogenic “brèche de Balène” between the Late Pliocene and the Mindel, according to Clauzon (1975). Dubar et al. (1978) considered alternatively that this same breccia was deposited after the thrusting episode and Dubar (1984), based on mammal biostratigraphy, concluded that the upper part of this breccia is post-tectonic. In its northern part (north of Saint Geniez), the Digne Nappe overlays the Authon-Valavoire

thrust sheet and the Barles half-window (Figs.1 and 2b) around which the basal thrust is folded in an antiform, allowing the outcropping of the Mesozoic series, and a synform represented by the Robine unit (Figs.1a and 2b) (Gigot et al., 1974). The Robine unit is now a distinct unit of the Digne Nappe, separated from the main part of the thrust sheet by the Bès dextral strike-slip fault (Gidon, 1997; Hippolyte et al., 2011). It is composed, according to a recent interpretation by Célini et al. (2020b), of three former NW-SE elongated transported mini-basins, the former salt walls now welded forming the contacts in-between. The Barles half-window represents the eastern part of the Authon-Valavoire thrust sheet (an intermediate unit between the Digne Nappe and the autochthon, Graham et al., 2012) (Fig.1b), with the Monges strike-slip fault in-between (Ehtechamzadeh Afchar and Gidon, 1974) accommodating strain partitioning within the sheet. The Robine unit bounds the Barles half-window to the south, and the main body of the Digne Nappe limits the eastern and northern edges of the window (Fig.1b). Graham et al., (2012) reinterpreted the Barles half-window as a separate allochtonous unit while most previous interpretations considered it as a part of the autochtonous series.

The Barles half window reveals some EW-trending folds affecting the Mesozoic series (resting unconformably on late Paleozoic metasediments to the north of Barles) and the first deposits of the Cenozoic Digne-Valensole basin in the south (Fig 2). Part of the Mesozoic folds formed in several stages, first in response to salt flow during the Jurassic with the Authon fold (Célini et al., 2020b), then in response to the Pyrenean and alpine shortening episodes. These folds were partly eroded and overlain by the Oligocene syntectonic continental deposits (Fig.1b), themselves folded by the Alpine phase and the Digne Nappe emplacement that tightened and overturned the pre-Oligocene folds (Haccard et al., 1989a).

In the south of the half-window, the deposits of the Digne-Valensole basin are dated from the Miocene to the late Pliocene and the basal continental Molasse Rouge and associated breccia are attributed, respectively, to the Oligocene and Eocene (Gigot et al., 1982; Antoine et al., 2022; Bialkowski, 2002). The sedimentation is marked by continental to marine facies transitions, evidenced by the succession of the continental Molasse Rouge, a lacustrine grey molasse and then marine molasses (Ford et al., 1999). The marine deposits (Fig.2a) begins with a thin transitional brackish molasse of the Aquitanian followed by the bird footprints-rich conglomeratic molasse of the Aquitanian-Burdigalian (Early Miocene) (Haccard et al., 1989a) (referred hereafter as m1-2 formation). This series is overlain by the marly and sandy molasses of the Burdigalian (referred hereafter as m2 formation), then covered by the Langhian Cerithes-

rich molasse (referred hereafter as m3 formation), known also as the Facibelle formation (Haccard et al., 1989a; Crumeyrolle et al., 1991). This molasse is fairly thin in the Velodrome area but shows a regional-scale erosive unconformity at its base (Crumeyrolle et al, 1991; Besson et al., 2005). Biostratigraphic constrains of the whole marine molasse are detailed in the supplementary data (1). This marine succession is then overlain by the Valensole Formation consisting of fluviatile conglomerates and alluvial fan deposits (referred hereafter as m4-p formation). The top of this formation consists of an olistolitic facies and according to some authors can be considered as a distinct formation with an erosive base (Tanaron formation) (Gigot et al., 1974; Haccard et al., 1989; Hippolyte et al., 2011). The age of this formation is still debated but its stratigraphic position at the top of the molasse basin just below the Digne Nappe makes it an important chronological marker. These points are detailed in the supplementary data (1).

This has however no impact on our modeling because we consider formations based on lithostratigraphic units rather than biostratigraphic units in the following.

The structural style and the dynamics of the Digne nappe remains debated in the literature. Recent studies show different interpretations of the deep structures. Balansa et al. (2022) show a continuous parautochtonous unit detached from a Palaeozoic basement thrust package above a decollement in the late Triassic evaporites. Halokinetic structures are only observed in the frontal part of the Digne Nappe (La Robine Klippe). Alternatively, Célini et al. (2022) favor a strong involvement of salt-tectonics from the Mesozoic to the Miocene, considering halokinetic structures in the Digne Nappe as mini-basins developed during the deposition of the Jurassic sediments. In the Digne nappe substratum, salt-tectonics is recorded from the Jurassic with the overturned Barre de Chine and Astoin megaflaps to the Miocene with the Vélodrome mini-basin. The large-scale fold uplifting the Barles half-window forms ahead of a thrust within the basement and is not transmitted at depth below the evaporite decollement level. Schwartz et al. (2017) show the succession of a first contractional stage with the southwestward propagation of the Digne Nappe over the Cenozoic foreland basin, followed by thick-skinned deformation of the Palaeozoic basement and long-wavelength folding causing uplift of the Barles window. These different interpretations at different scales denote drastically different visions of the role of the viscous evaporites in the construction of the foreland-and-thrust belt with similar geometries at the surface.

The whole succession of those Tertiary formations is folded, presenting a complex 3D plurikilometer syncline, the so-called Vélodrome. The Vélodrome is described as a recumbent fold with a curved axis bent from EW in the north to NS in its eastern part (Fig.3). The Vélodrome is bounded by the folded Mesozoic series and the Digne Nappe, to the north and the south, respectively. On the western side, the Monges strike-slip fault dies out toward the south and another Miocene overturned syncline is observed beyond its southern termination, the Melan-Auribeau syncline that could be the western extension of the Vélodrome offset left-laterally by distributed strike-slip deformation, but this is not ascertained (Fig.1b) (Gigot et al., 1974). Several mechanisms of development have been proposed for the Vélodrome. It has been classically interpreted as a syn-sedimentary fold related to the development of the fold-and-thrust belt (i.e. as a growth fold) (Gigot et al., 1974; Gidon and Pairis, 1988; Haccard et al., 1989a; Gidon and Pairis, 1992). The Vélodrome has alternatively been considered as a post-sedimentation fold resulting from the Digne Nappe emplacement and the latest Alpine movements (Fournier et al., 2008). More recently, it was proposed that the Vélodrome formed as a salt-controlled mini-basin in relation to an allochthonous salt sheet emplaced during Miocene at the tip of the thrust sheet (i.e. thrust-fed salt sheet) (Graham et al., 2012; Célini et al., 2022). This debate reveals a lack of consensus on the internal structure of the Vélodrome, more specifically on the existence of internal unconformities and the potential role of salt motion. A high-resolution structural study is proposed here in order to precise and model the internal 3D geometries between and inside the Tertiary formations (i.e., potential presence of unconformities and their spatial distribution).

3. Approach

3.1. 3D geometrical modelling approach

3.1.1. Geomodeller modelling principles

3D geometrical modelling approach is well adapted to test hypotheses and image complex non-cylindrical geological structures in detail (Calcagno et al., 2008; Do Couto et al., 2015; Saspiturry et al., 2022). Generally, two main approaches in 3D geometrical modelling are available for modelling geological interfaces (see Frank et al., 2007; Collon et al., 2016) : (1) the implicit approach considering geological interfaces as isovalues of a 3D scalar field, and (2) the explicit approach that consists in building meshed surfaces that fit available data. Implicit modelling methods present the advantages to automatically prevent overlapping issues, to be

more suitable in a context of sparse data set, and to request a shorter processing time that facilitates the addition of new data and an iterative 'trial and error' process, mainly by alleviating mesh processing requirements. On the other hand, explicit approaches offer a better control on the topology of the resulting interfaces, which can prove useful for managing the segmentation and relationships of the different parts of a model (Collon et al., 2016). In our case study, this clearly presents a lower interest compared to the flexibility offered by the implicit approach. In this study, we used the implicit 3D modelling software package Geomodeller (© BRGM – Intrepid Geophysics), in which 3D geometries (geological surfaces and bodies) can be interpolated and directly visualized between data points.

The Geomodeller is based on the interpolation of a pseudo-potential field method (Lajaunie et al., 1997) where (1) one geological boundary is considered as one isovalue surface from this potential field and (2) the structural measurements (either bedding or foliation depending on the geological context) as oriented measurements of the pseudo-potential field gradient vector. This potential field is thus defined by a scalar function T(p) calculated at any point p(x,y,z) of the 3D space considered. Any point p for which $T(p)=t_k$ belongs to an isopotential surface representing the value t_k of the potential field (Calcagno et al., 2008). Each potential field is computed from geostatistical parameters (range, nugget effect, and drift degree) corresponding to the natural correlation tendencies between data points. The T function represents a geological event such as the deposit of a sedimentary formation or the emplacement of an intrusion. Isopotential surfaces can also be considered as isochrone surfaces (Calcagno et al., 2008) within a sedimentary series. Technically, one scalar function (one pseudo-potential field) is calculated for each 'coherent package of geological units' (called *series* here after (Calcagno et al., 2008)), which can be a single sedimentary formation or several successive ones showing consistent continuous deposition conditions.

The method requires input data for the interpolation of an interface, namely: (1) the X, Y, Z coordinates of at least one point localized along the corresponding interface, (2) at least one orientation data for each *series* and (3) the indication of the polarity. It is noteworthy that (1) orientation data do not necessarily have to be measured along the interface and can be introduced anywhere within the modelled geological *series*, and (2) each unit will benefit from the orientation data from other units in the same *series* as they are described by the same scalar field, although being defined different isovalues.

3.1.2. Managing unconformities

During the modelling process, sedimentary units are organized into a *geological pile* constituted of *formations* bundled into *series*. *Series* are successive formations sharing a common evolution, grouped together. The same scalar function (and also the same set of geostatistical parameters) is used to interpolate all formations belonging to the same *series*. Formations in a *series* are thus considered conformable (Fig.4a). Then, the interpolation of two unconformable formations is conceivable only if the formations belong to two different *series* (Fig.4b and c). If strata orientations are oblique from one *series* to the other, this option will result in an unconformable contact in between. If strata are parallel, no unconformable strata will be forced.

In this study, two *geological pile* settings are tested in order to discuss the presence or absence of unconformities in the sedimentary units, allowing to test the syn- or post-sedimentary folding hypothesis in the development of the Vélodrome structure.

For the modelling sequence, *series* are defined by their geometrical 'behavior', either 'erode' or 'onlap', relatively to the *series* already interpolated in the modelling sequence (from bottom to top; Fig.4b and c). An 'erode' option allows a *series* to crosscut another *series* previously computed and thus affects computed volumes of the lower *series* in the stratigraphic sequence (e.g., used in a context of an erosive episode or a basin sedimentary filling knowing a deceleration of subsidence) (Fig.4c). Conversely, a *series* with an 'onlap' behaviour does not formerly modify interpolated *series*; the 'onlap' *series* is only interpolated in the remaining empty volume of the entire 3D space (e.g., used in a context of a basin sedimentary filling recording an acceleration of subsidence) (Fig.4b). In this study, the *geological pile* has been defined to compute the sedimentary formations according to the stratigraphic depositional sequence, from the oldest to the youngest one. Concerning the behaviour between different *series*, the 'onlap' behaviour option has been systematically chosen between different *series* of the Miocene units of the Vélodrome, according to the increased rate of subsidence observed in the region (Couëffé and Maridet, 2003).

Moreover, it must be mentioned that, in Geomodeller, thicknesses of the sedimentary formations are not defined as input parameters of the model. The only way to fix thicknesses is to systematically add manual constraints along cross sections, for instance. Thus, resulting thickness variations within one formation in the model can be interpreted either as real lateral thickness variations or as progressive unconformities of the strata within the given formation. The only way to consider progressive unconformities within units would be to split them into

series containing a single formation, which would necessitate very high resolution of both contacts and structures orientation measurements.

3.2. Data set and field analyses: from field to virtual outcrops

The modelling process is based on going back and forth between field observations and analyses on the one side, and modelling sessions on the other. Based on structural data, the modelling approach requires a data set as detailed as possible. Because preliminary calculations showed the pre-existing data set was not dense enough, several field campaigns were conducted to complement it and a total of 2328 new structural orientation measurements (strike and dip) were made in the Vélodrome formations (Fig.5). Field observations and measurements were realized both *in situ* with a compass (2100 measurements), and indirectly by drone images (Dji Mavic pro and Dji Phantom 3 pro) using photogrammetric models. In these models, the orientation of structural surfaces was calculated where not directly accessible on foot (228 measurements) (Fig.5). We used Metashape (Agisoft) and LIME software for SfM photogrammetry processes (e.g, Westoby et al., 2012) and orientation measurements (Buckley et al., 2019), respectively.

In addition to the requirements for a dense data set, the overthrust of the Digne Nappe on the Vélodrome makes potential unconformities smaller scale objects only observable thanks to local oversampling. Then, in order to identify the inter- and intraformational geometries within a single limb of a fold, detailed dip profiles were acquired perpendicular to the average strike of formations and to fold axial surfaces. All bedding measurements are plotted in a maximum 170 meters wide swath profile and systematically belong to the same limb of a fold. Far from a fold hinge, the absence of dip variation along the profile would exclude the presence of significant internal unconformities. Closer to the fold hinge we add an expected theoretical model to compare the theoretical dips of the fold to those measured.

4. Field analysis

4.1. Overall Vélodrome structure

Five cross-sections (3 NS-oriented and 2 EW-oriented sections – Fig.5) built from the published map (Haccard et al., 1989b) together with new field observations are presented on Figure 6. The first cross-section (section 1 - Fig.6) - north-south oriented - displays a complete overview of the Auribeau recumbent syncline north of the Vélodrome, whose overall structure is tilted to the south. Vertical to totally overturned beds are observed toward the north with 20

to 25° reverse northward and southward dip in the m1-2 formation (Fig.5). We infer that these overturned beds prolongate southward, under La Coustagne and La Fubie, according to the observed overturned beds further east (Fig.3, 6 – section 3 and 7c and d). The recumbency is also observed in the red marls of the Valensole formation, under La Fubi, where both the lower and upper limbs of the fold can be observed (Fig.8 and 9). Furthermore, the recumbent geometry of the fold is particularly well exposed in the western part of the Vélodrome (west of La Coustagne) were overturned m1-2 layers form an ~E-W trending antiform showing 20° reverse dips to the north, to 30° to the south (Fig.5). Section 1 also highlights the tightness of the Auribeau and Bès synclines in the extremity of the structure as well as the anticline in the center. Two klippen in the north can also be observed on top of the overturned beds. The first klippe corresponds to a detached piece of m1-2 (known as La Fubi) lying directly on overturned red marls and conglomerates of the Valensole Formation through a tectonic contact (Haccard et al., 1989a), often interpreted as a Digne Nappe-related thrust (Figs. 8 and 9). Red marls display short-wavelength folds just below this tectonic contact, and minor normal faults are visible in the molassic deposits above the thrust (Fig.8). The La Fubi outcrop forms a recumbent fold with a largely exposed normal limb at the base, on top of the thrust contact, and a partly eroded reverse upper limb. Structurally above the La Fubi unit and located more northward, another Digne Nappe-related thrust transported beds of the upper Jurassic succession (the so-called La Coustagne unit) (Fig.9). The Jurassic beds are folded and lie on the overturned m1-2 formation of the overturned limb of the Vélodrome (Figs.8 and 9).

On section 2, 1500m eastward (Fig.6), one can observe the same overall structure of the Auribeau and Bès syncline. The tight feature of the Auribeau fold is observed at short distance west of the sub-vertical layer of the cerith-rich Langhian formation m3 (so-called Lame de Facibelle), in the fluvial deposits of the Valensole formation (Fig.10a). Rheological contrasts of the Vélodrome series allows the formation of small disharmonic folds such as the Ubac anticline observed in the core of the fold (Fig.5). In this area, one can identify a dip variation into the m2 molasse which swings from 75° with a normal polarity to the south at the top of the formation, up to 82° reverse dip to the north at the base of the formation further north (Fig.12c). The transition between the m2 and the m1-2 is marked by an angular unconformity as the m1-2 layers show 65° in average reverse dip to the north (Fig.5). The Auribeau syncline is bounded to the south by the Digne Nappe thrust, associated with Triassic gypsum layers. In the northern part of the section, the m1-2 layers are deposited on the Oligocene continental molasse and the Eo-Oligocene breccia (composed by vertical deposits lying on the Mesozoic series) or onlap directly the Mesozoic carbonates (Fig. 5). To the south, the upper part of the Valensole

formation is covered by chaotic facies (Tanaron Formation, Fig.7b and d) constituted of Jurassic and early Cretaceous calcareous blocks, red marls and conglomerates. In the literature, the Tanaron Formation has been interpreted either as a lateral equivalent of the upper Valensole (Gidon and Pairis, 1988) or a younger unit incising the Valensole formation (Haccard et al., 1989a; Hippolyte et al., 2011).

Cross-section 3 is located in the eastern part of the structure (Fig.6), showing also the succession of Auribeau and Bès folds overthrusted in the south by the Digne Nappe. At the southeastern edge of the Vélodrome, near Esclangon, the overturned m1-2 layer oriented N075-57° dips to the south (Fig.3) testifying for the abrupt closure of the fold in the south, with the Bès overturned syncline, which axial surface dips to the south (Figs.6 and 7). The abrupt feature of the Bès syncline is associated with the pinching of the formations and successive unconformities into the m1-2 and m2 formations (Figs.5 and 7). This geometry, proposed by Célini et al. (2022), is however not consensual and the geometry of the Bès syncline near the village of Esclangon should thus be further discussed, because its precise geometry is complex.

Classical interpretations show a fold with a N-S axis that acquired its southward dip only after the long wavelength folding episode that affected the whole region, including the basal contact of the Digne Nappe (Gigot et al. 1974; Crumeyrolle et al., 1991; Gidon & Pairis 1992). In this region, the m2 beds dips toward the southwest where clear internal unconformities are observed, showing that the fold axis is neither strictly N-S nor E-W. It locally dips toward the SW as also suggested by its geometry on the map. The internal unconformities suggest that the fold was formed progressively during sedimentation. The whole structure was then tilted toward the south after the southward overthrusting of the Digne Nappe by a late folding of the nappe contact and its substratum. Two stereographic diagrams (Fig.11) show the attitude of the molasse beds in their present position and in their pre-tilt position. Back-tilting consists here of substracting the late long wavelength folding of the Digne Nappe about an E-W axis. Orange planes correspond to the m1-2, green ones stand for the m2 and black ones for the m3. Two observations can be made. (1) The intersection of bedding planes occupies a large zone of the diagram, showing that the fold strongly departs from cylindricity. It obviously has a N-S component, but the observation of the map and panorama photo (Fig.7c and d) shows that it also has an E-W component, which is confirmed by the stereograms. (2) The m1-2 and m2/m3 bedding planes are clearly separated on the diagram, showing a clear bi-modal distribution. This observation can be explained by (a) the progressive unconformities in the two main formations and (b) by the fold. We think that the main reason is the unconformities because of

the apparent oblique direction of the fold axis on the map. The conclusion is then that the very loose intersection of bedding planes on the diagram shows the approximate position of the intersection in space of the bedding planes of the upper and lower formations due to these internal unconformities rather than the fold itself that is not cylindrical. The fold that cannot be simply treated with such diagrams because of its strong departure from cylindricity. This conclusion further suggests that the Bès fold partly postdates the deposition of the m2 formation. We thus conclude that the direction of the fold axis is oblique and curved in this region from a N-S direction in the north to a more E-W direction in the south (Fig.11). In the following we however test two situations, one with the north-vergent fold prescribed and one where no such constraint is imposed.

Moreover, in the center of the cross-section, the incision of Bès river reveals the EW-oriented Martellet anticline involving the whole Miocene series (Figs.3, 5, 6 and 7b). This anticline is only observable in the east due to its upward damping. Thus, the younger the series, the less deformed they are. Moreover, this fold also disappears eastward under the Esclangon ridge.

Looking at the Vélodrome structure on EW-oriented sections (Fig.6 – sections 4 and 5), it displays a gently and regular westward dipping monocline of the molasse with an abrupt north-south striking syncline at the eastern extremity of the structure (Esclangon fold) (Fig.1b). The Esclangon fold shows a gently west dipping axial surface and 68° in average reverse dip for the upper limb (Fig.3, 10b and c). The western part of cross-section 4 highlights the lower and upper limbs of the Auribeau fold in the Valensole formation under the La Fubi klippe, itself displaying a recumbent fold. To the west, the Vélodrome is also bounded by the Digne Nappe thrust associated with the Triassic gypsum deposit, and in the east by a large outcrop of Oligocene Molasse Rouge, itself overthrusted by the Digne Nappe. Lastly, cross-section 5 is located 500 meters further south where one can also observe the Esclangon syncline. This section shows a dip variation of the m2 layers as we approach the Esclangon syncline with dip varying from west to east from 62° normal to 87° reverse (Fig. 7e and f).

4.2. Fold geometries

As for the folds, in the north of the Vélodrome, the Auribeau syncline is a syncline with the shape of a basin with steep walls on three sides at least, north, east (Esclangon) and west (Lambert) involving some lower Miocene to upper Miocene-Pliocene formations. The axis (measured in the m4-p), plunges 33° to the N282°E, and the axial surface is oriented N084-64N

(Fig.10a and c). In the east, between old Esclangon and cross section 5, the Esclangon syncline axis dips 09° toward N330°E and its axial surface is oriented N313-30E (Fig.10b and c). In the southeastern part of the Vélodrome near Esclangon, Miocene beds form the Bès tight syncline that is not cylindrical (Fig.5 and 11). The Bès fold axis is oblique and curved in this region from a N-S direction in the north to a more E-W direction in the south (Fig.11). These last two folds can be considered either as one single fold with a curved axis (Fig.5) or as two distinct folds. Lastly, in the eastern area near the Bès river, Miocene beds form an anticline with an axial surface oriented N106-81N and a subhorizontal axis (08° to the W) plunging toward N288°E (Fig.5). Internal geometries described below allow precising the timing of folding episodes.

4.3. Geometries of Vélodrome beds

In the northern part of the Vélodrome, the molasse sedimentary series displays two different inter- and intraformational geometries. Figure 12 shows detailed dip profiles within fold limbs. The m1-2 molasse displays monoclines for sections of about 200 up to 350 m of apparent thicknesses (Fig.12a, b, d) with one reverse monocline dipping 58° to the north (section d), and two others of respectively 74° (section a), and 52° normal dip (section b), to the south. In contrast, dip profiles in the m2 layers highlight progressive dip variations (section c, 350 m long - Fig.12) from 70° normal dipping to the south, at the top of the series, to 80° reverse dipping to the north, at the base. In addition, the connection between the sections c and d (Fig.12), corresponding roughly to the contact between the m1-2 and the m2 molasses, shows a 20° dip change (Fig.12). We interpret this dip change as an unconformity between the m1-2 and the m2 molasses. This value is perhaps overestimated because both merged sections are slightly offset due to outcropping conditions. To the south, the same unconformity between m1-2 and m2 is present, highlighted by onlaps visible both on the map (Fig.7) and in cross-section, thanks to the subvertical pattern of Miocene beds in this zone. In the m2 near Esclangon village (section e, 65 m long – Fig.7e and f), we note a transition from reverse dips around 87° to the east, at the base of the formation, to ~63° normal dips to the west in layers structurally above.

5. 3D geometrical modelling results

5.1. Vélodrome model settings

The Vélodrome 3D model covers a surface area of about 25 km² (~6500 m per 3800 m) with an altitude varying from -500 m to 1680m. The sedimentary pile includes series from the

Early Miocene (Aquitano-burdigalian) to the Late Miocene or Pliocene (Valensole conglomerates).

Here, we use the 3D modelling of units as formations and *series* to test contrasted hypotheses for the development of the Vélodrome structure. Two models with two end-members set-ups are presented (Fig.13). The first model involves a post-sedimentary folding of the series; it has thus been computed with six formations bundled into one single *series*. The second model corresponds to a synsedimentary folding hypothesis and is computed with six formations organized into six *series*. The large amount of data in the Burdigalian unit allows us to split it into 3 *series* in the second model in order to unravel possible internal progressive unconformities within this unit.

La Coustagne unit and La Fubi unit are considered as separate units, and the Tanaron unit (labelled hereafter in the model) is separated from the Mio-Pliocene units of the Vélodrome. In some works (e.g., Gidon and Pairis, 1988), the Tanaron Formation has been considered a lateral facies of these Mio-Pliocene formations that we cannot introduce in the model. The Tanaron unit is thus computed as a *series* whereas La Coustagne and La Fubi units are grouped in the same formation and the same *series*.

The models are both based on:

(1) a 25 m resolution Digital Elevation Model (DEM) from IGN (©IGN, 04-2015),
(2) 2328 bedding orientation measured data points (2100 field data, 228 extracted from photogrammetric models realized from UAV image),
(3) structural orientation interpretation data (from field interpretations or extrapolated observations, in case of outcrop lacking): 160 points for the postsedimentary hypothesis and 40 points for the synsedimentary one. These interpretation data points are directly added into sections.
(4) coordinates of points extracted along the interface surfaces between formations (observed in the field and extracted from existing geological maps): 409 points for the postsedimentary hypothesis and 822 for the synsedimentary one. These data points are directly loaded in the sections.
(5) a set of common geostatistical parameters defined for each *series*:

- 1800m for the range (half of the smallest side of the model box),

- 2 for the drift degree, allowing a second order polynomial of space coordinates as a drift function, which is the most suitable for uncylindrical fold structures (and the least constraining from a geostatistical point of view),
- negligible (0,000001) nugget effect applied both to the coordinate values of the points along the interfaces and to the structural orientations. Large nugget effects are often used in this approach in order to smooth and simplify the interpolated geometries by allowing the model not to strictly pass through the points or tangent the measured structural angles. Here, instead, the large density of measurements allows us performing interpolation with no smoothing or simplification of the individual local data.

5.2. Constraints imposed to the model

In addition to field measured data, the modelling process requires additional constraints where (i) density of data is insufficient (zones of outcrops lacking) or where (ii) structure is changing too quickly with depth. Some orientation data and interface points are thus added into sections of the 3D model (topography and vertical ones) and, among those constraints added, two types emerge: (i) direct interpretative constraints associated with field observations extrapolated from reference zones and used for both models, and (ii) indirect interpretative constraints derived from the tested hypothesis that differ from one model to the other. In the absence of geophysical data, the process of adding constraints has been realized only from surface data.

5.2.1. Direct interpretative constraints

In a field data acquisition campaign, the data distribution is heterogeneous due to the occurrence and quality of outcrops. The model box thus displays (i) areas with a data density consistent for all the formations called reference zones and (ii) areas with a poorer data density (Fig.14a). Each type of zone will require a different modelling approach.

Approach for data-rich areas

The eastern area is well constrained by the measured orientations due to the outcrop quality in 3D (Fig.14a) and does not necessitate significant interpreted constraints. This data-rich area is interpolated essentially on the base of the structural data with a minimum of input points located along the interface. The large density of measurements in this area allows us — with a negligible nugget effect and a minimum of contact points — testing whether the interpolation fits well the geological boundaries drawn in the map (Haccard et al., 1989b).

Approach for data-poor areas

The western part of the Vélodrome includes data measured exclusively within the Lower Miocene m1-2 formation (Fig.14a), making it a data-poor area for other units and thus necessitating the input of additional data. In the whole northern part of the Vélodrome, from La Chapelle to Lambert, (i) the basal Lower Miocene m1-2 formation displays a roughly cylindrical structure, and (ii) its eastern part includes a high data density for all formations from the Early Miocene to the Pliocene (Fig.14a). Thus, the northeastern part of the Vélodrome represents a reference zone (reference zone 1) from which the northwestern part will be constrained by projection. In the same way, the southeastern part displays a large amount of detailed data (reference zone 2) which is projected to the west. Maps of the reference zones are displayed in Fig.14a.

The following points synthesize the main elements observed in the reference zones that will be projected in the data-poor area:

(i) The Auribeau syncline characteristics, i.e., the WNW 30° plunging axis and the interlimb angle of 70° (Fig.10a and c and 14c – section 1).

(ii) The north verging recumbent Bès syncline (Fig.7, 11 and 14c – section 2).

(iii) Measured sedimentary formation thicknesses (synthesized in Fig.2) are respected in the core of the map-scale structure (i.e., within the lower limb of the fold) (Fig.14c – section 1).

(iv) The relative obliquity angle between formations as measured in the limb of the Auribeau syncline exposed in the north (area between La Coustagne and La Chapelle) (Fig.14c – section 1).

5.2.2. Indirect interpretative constraints

The model testing the postsedimentary folding hypothesis involves parallel interfaces between units and preservation of formations thicknesses according to a (sub)horizontal deposit of the successive Miocene sediments. Following this point, and according to the recumbent feature of the Vélodrome observable in the west, the western part of the model must display the double layer thicknesses for the lower and the upper limb of the fold. The interpolation by pseudo-potential field method does not ensure thicknesses preservation, thus points along interfaces are systematically added to fix thicknesses and thus testing the postsedimentary folding hypothesis.

On the other hand, the model testing the synsedimentary folding hypothesis is mainly based on the onlaps both of the Burdigalian m2 layer on the top of the Aquitanian-Burdigalian m1-2 and into the Burdigalian, observed both in south and north of the structure that will be projected in data-poor areas.

5.3. Vélodrome models and interpretations

5.3.1. Post-sedimentary hypothesis

This first model has been computed using one single *series* composed of six formations (one for the Aquitano-Burdigalian m1-2, three for the Burdigalian m2, one for the Langhian Facibelle formation m3, and one for the Late Mio-Pliocene Valensole formation m4-p), excluding the construction of unconformities between formations (Figs.13a, 15a and 16a).

The result of 3D geometrical modelling (Fig.13a) reproduces fairly well most of our field observations, especially for the near-surface and eastern parts of the structure. It includes: (i) the recumbent pattern of the Vélodrome structure in almost all directions (east, north, and west); (ii) the tightness of the fold both in the younger formations in the Facibelle area and the southeastern part near Esclangon; (iii) the change of bed strike in the marine molasse, including the closure of the Vélodrome in the southeast part; and (iv) the anticline in the core of the Vélodrome with a declining influence toward the west.

While the overall geometry is partly well interpolated, constraints derived from the post-sedimentary hypothesis implies that the base of the Valensole formation is at around 1600 m depth in the western part of the model (Fig.15a). Such consideration would imply a localised vertical offset of 775 m of the base of the basin between its eastern and western parts (Fig.15a). This offset requires consequently a vertical fault outcropping just east of La Coustagne. However, field observations indicate a lateral continuity of the m1-2 and m2 molasse and its outlines are clearly continuous in the map. No evidence of such localized structure is visible at the surface or has ever been reported, neither in the Vélodrome Miocene molasse nor in the north in the Mesozoic series structurally beneath.

5.3.2. Syn-sedimentary hypothesis

The second model is computed based on one *series* defined for each formation, it then comprises six *series* for six formations including one for the Aquitanian-Burdigalian m1-2, three for the Burdigalian m2, one for the Langhian Facibelle formation m3, and one for the Upper Miocene-Pliocene Valensole formation m4-p. Such model configuration allows the

interpolation of unconformities between formations (between *series*), but without forcing them (Figs.13b, 15b, 16b, 17 and 18).

As for the first model, the overall geometry of the structure (described above) is well reproduced by the result of the 3D geometrical interpolation modelling (Figs.13b and 18). This second model further results in unconformities between all formations, reproducing local field observations (e.g. onlaps in m2 near Esclangon) (Figs.15b, 16b and 17).

The result of this 3D modelling (Figs.15b and 17a) does not imply, contrary to the first model, any step of the basin's basement through the Vélodrome and conversely highlights a continuity of the bed attitudes at depth from east to west. Indeed, unconformities could be here associated with fan-shaped deposits in a syntectonic basin setting involving thickness variations and especially thickness decrease toward fold hinge. This pinching shape of the extremities of formations (Fig.16b) opens a space in the upper limb of the recumbent fold (Fig.15b), allowing the continuities of layers at depth, with no deepening interpolated of the base of the basin in the western part of the model.

In order to test the geometrical compatibility with field measurement and the geological map of the classical interpretation of the Bès fold (Gigot et al. 1974; Crumeyrolle et al., 1991; Gidon & Pairis 1992), we have also modelled the southern part of the Vélodrome without imposing the north-verging fold (Fig 19). The result shows that the field measurements of bedding strikes and dips and the geological contours alone are sufficient to generate a fold with an ENE-WSW axis, overturned toward the north, in agreement with the analysis of stereograms described above (Fig.11 and 19). The Bès fold, overturned toward the north, thus appears in the model with or without imposing it on the cross-sections, showing that it is a robust hypothesis.

6. Discussion

6.1. 3-D geometry of Vélodrome units

A thorough study of the internal strata geometries allows us recognizing different timings and deformation histories within the Vélodrome fold with two distinct zones in the north and in the southeast.

In the north, from a distance, panoramic views on the beds of the Aquitanian-Burdigalian m1-2 molasse apparently suggests fan shape type deposits (Fig.12e). However, the high-density structural measurements set produced in this study clearly highlights parallel strata

in this part of the basin and does not indicate any internal unconformities into the Aquitano-Burdigalian sedimentary formation, north of the Vélodrome structure (Fig.20). Even though we cannot entirely exclude the previous presence of syn-sedimentary structures that are currently not present, we suggest that, at that scale, these molassic layers were deposited horizontally with a uniform subsidence not controlled by any local tectonic structure. This further implies that deformation of the basin necessarily begun after the early Burdigalian.

In contrast, a detailed bedding orientation profile made within the m2 strata (Fig.12c) clearly highlights continuous dip variations in this upper series. Such internal dip variations could be attributed to the nearby map-scale fold hinge zone of the Auribeau syncline along the basin edge, but a simple simulation of an isopach fold does not account for the entire 30° fan angle range measured in the field (Fig.21a) and internal unconformities can be proposed. We thus had a further look at the onlaps described by Crumeyrolle et al. (1991) near Col d'Ainac based on the interpretation of satellite images (Google Earth, 2004 image). Figure 21b shows the contours of the La Javie 1/50 000 geological map, only slightly modified, and the geometry of beds in the m1-2 and m2 formations. The obliquity of m2 layers and their onlapping geometry in the reverse limb of the Auribeau overturned syncline equivalent are clearly visible, confirming the drawings of Crumeyrolle et al. (1991). The bedding dip variations we measured in the Burdigalian m2 molasse are thus fully compatible with these progressive onlaps and wedgings first described by Crumeyrolle et al. (1991), and which can be interpreted as a combination of syn-tectonic features and eustatic unconformities. As for the youngest formations, 3-D modelling results (Figs.15b, 16b and 17) highlight obvious unconformities from the m2 to the Valensole Formation. Thus, our data and modelling results confirm the syntectonic character of the Vélodrome formations from the Middle Miocene to the Late Miocene- Pliocene in the northern part of the Vélodrome.

In the central part of the basin, at the scale of our model, as proposed by Fournier et al. (2008), 3-D modelling does not show any internal unconformities in this area corresponding to the lower gently dipping limb of the Vélodrome map-scale fold. Local internal unconformities have however been described within the Facibelle formation and overlying continental marls and sandstones (noted m3-5 and m5-p on La Javie 1/50000 sheet) but they are of too small scale to appear on the 3-D model.

In contrast, the southern and eastern parts of the Vélodrome structure are characterized by strong thickness variations observed within the m1-2 layers (Fig.22), with a sharp and systematic thinning of all the constituting layers from north to southeast. Here, the fan shape

structure observed in photogrammetric model views (Fig.7c and d) clearly corresponds to a continuous change of bedding orientation. The abrupt thickness variations, the unconformable geometries in the younger formations around, and the 3D modelling results highlight internal unconformities within the m1-2 formation in the southeast with pinching of this formation toward the south, implying synsedimentary deformation. We also note some slight onlaps onto the Oligocene molasse as also mentioned by Crumeyrolle et al. (1991) indicating the filling of a paleotopography and/or an eustatic change during Aquitanian times. The m1-2 syntectonic deposits and onlaps onto the Oligocene molasse are probably due to differential subsidence induced by an uplift located southward starting in late Oligocene-early Miocene times.

At the scale of the Velodrome, the internal unconformities in the m1-2 formation in the south and their absence in the north show that deformation started earlier in the southern area, as soon as the Aquitanian. As for the northern part, internal unconformities are clearly observed in the Burdigalian series in the southeast (Fig. 7d) as also testified by the variations observed in the structural measurements extracted from the photogrammetric drone data (Fig. 7e and f). Such feature attests for the persistence of tectonic movements up to the Burdigalian over the entire Vélodome area. Finally, our modelling results confirm and extend the occurrence of unconformities in the whole southern half of the Vélodrome (Fig.17).

The deformation in the Vélodrome is then diachronous as suggested by Gidon and Pairis (1992), with onset during Aquitanian (m1-2) in the south and southeast, and during the Burdigalian (m2) further north. At first sight, the Vélodrome syncline can be described as a single fold with a curved axis. However, the asynchronous deformation seems to support the occurrence of two or more isolated folds (Fig.22). Moreover, due to the continuity of bed orientations on either side of the Bès river, it is impossible to draw a single axial surface accounting for the NS- and the EW-oriented beds. Thus, we interpret the Vélodrome as an interference between two or three different folds formed at different times, possibly associated with different processes (Figs.5 and 10). We furthermore suggest that the southern tight EW-oriented Bès syncline, which bounds the Vélodrome to the SE, continues to the west until Lambert village area under the Digne Nappe (Fig.13). The westward dip of the m1-2 in the westernmost part of the fold at the west of Lambert supports this interpretation.

6.2. Deformation mechanisms of the fold

6.2.1. Not a simple 2D growth fold

The Vélodrome structure is commonly interpreted as a growth-fold with sedimentary onlaps and progressive unconformities (Gigot et al., 1974; Gidon and Pairis, 1988; 1992; Haccard et al., 1989a; Crumeyrolle et al., 1991; Lickorish and Ford, 1998; Balansa et al., 2022) probably associated with the activation of the Digne thrust front further northeast (Lickorish and Ford, 1998). Timing of the activation of the thrust front in the Barles area has been proposed to date from the Oligocene (Balansa et al., 2022), the Early Miocene (Gigot et al., 1974), or at the end of marine Miocene deposition (Gidon and Pairis, 1992; Lickorish and Ford, 1998) based on the transition from marine molasse to continental coarse conglomerates. Our detailed analysis of Miocene strata orientations and our 3D geometrical modelling results shows respectively strictly conformable Aquitanian-Burdigalian (m1-2) strata in the north and evidences of synsedimentary tectonics only starting during the Burdigalian (m2molasse). Thus, our new results in the north of the Vélodrome agree with the growth-fold hypothesis and precise the timing of deformation. Although the final geometry and the involved layers tend to show that the Vélodrome fold largely developed during the deposition of the Valensole Formation, we propose that Burdigalian synsedimentary structures of the northern part evidence early far-field effects of the Digne thrust front during this period. The far-field activation could have been accommodated by the growth of other local well-known folds north of the Vélodrome in the Mesozoic substratum. These processes may have controlled the development of growth strata in the northern part of the basin during Miocene times (e.g. Pairis and Gidon, 1987, Balansa et al., 2022).

The obliquity between the EW strike of Auribeau syncline axis and the SW displacement direction of the Digne Nappe (Lickorish and Ford, 1998; Aubourg et al., 1999; Graham et al., 2012; Balansa et al., 2022) suggests either a strong inheritance of E-W structures developed during the earlier Pyreneo-Provençal episode (Lacombe and Jolivet, 2005) or a deformation partitioning between a SW-directed thrusting and a dextral strike-slip component (Lickorish and Ford, 1998), or a combination of both.

To explain the NS fold axis in the eastern part of the Vélodrome, Gigot et al. (1974) suggest the superimposition of an inherited dextral strike-slip structure creating a torsion of the Vélodrome fold axis near Esclangon. The occurrence of dextral strike-slip structures known in the region (Gigot et al., 1974; Lickorish and Ford, 1998; Fournier et al., 2008; Hippolyte et al.,

2011; Balansa et al., 2022) supports this hypothesis. Furthermore, we can image a complex geometry of the Digne Nappe decollement as sloping ramps that could lead to the formation of NS-oriented folds. However, the NW vergence of the Bès syncline cannot be compatible with the displacement to the SW of the Digne thrust front.

6.2.2. Result of several successive shortening events?

The Vélodrome displays at least two distinct folds (the Auribeau and the Esclangon fold) suggesting two different folding directions. A way to integrate both the EW-oriented Auribeau syncline and the NS-oriented Esclangon syncline could be to consider the Vélodrome as the result of interference of folds with a first shortening episode ranging from N-S to NE-SW followed by an oriented shortening event ranging from E-W to SE-NW. However, this study shows that the NS-oriented Esclangon syncline formed first, which rules out the hypothesis of a succession of shortening events beginning with a NS to NE-SW shortening direction. Furthermore, if the S-SW shortening direction episode can be considered consistent with the displacement direction of the Digne Nappe, no regional-scale tectonic event can stand for E-W or NW-SE-oriented shortening in the Digne-Valensole area. Moreover, such a significant deformation stage would produce other N-S structures in the Velodrome than the single Esclangon fold.

Furthermore, another hypothesis implying several shortening events is to involve a N-S trending tectonic accident with a W or NW vergence, which would now be hidden under the Digne Nappe and at the origin of the Esclangon fold, as Gidon and Pairis (1992) proposed. This fault would have been active since the Burdigalian or even the Aquitanian in the light of observed and suggested unconformities or layer thickness changes in the field and the 3D geometrical model (this study). The occurrence of a N-S trending thrust observed into the Oligocene near the old Esclangon suggests also the occurrence of such a structure below the Digne Nappe. This additional tectonic unit often named “Ecaille d’Aiguebelle” (Gidon, 1989), essentially made of the red molasse, resting on top of the eastern limb of the Vélodrome and beneath the Digne Nappe. This unit wedges northward and disappears between the Digne Nappe and the parautochtonous units of the Barles half-window north of le Ravin du Rousset. We did not make any attempt to include it in the 3D model because the uncertainties on the geometry of the lower and upper contacts, in terms of position and dip, are too large.

The presence of this unit would be moreover compatible with the occurrence of several N-S faults observed in the Digne area (Monges, Frayssinie, and Bès faults). A WNW-ESE compression episode has also been documented by Fournier et al. (2008) that supports the influence of such a structure, the origin of which is so far unknown and we cannot totally rule out some east-west movement of the Digne Nappe more compatible with such a N-S striking fault. Whatever the hypothesis invoked to consider several shortening events, none explains the Bès fold overturned to the north. It does not explain either the contemporaneity of the E-W and N-S striking folds in the m2 molasse.

Further south, in the Valensole basin, the Aiglun and Mirabeau-Mallemoison anticlines (Fig.1a) also display two different fold axis directions in the north and in the east. The NW-SE fold axes seem to rotate eastward to a N-S oriented anticline, as shown by the fold hinge reported in the 1/50,000 geological map of the Digne area (Digne sheet numb. 944, Courtillot et al., 1981) and Forcalquier (Forcalquier sheet numb. 943; Thomel et al., 1982). The Aiglun and Mirabeau-Mallemoison anticlines formed during the Late Pliocene-Quaternary times, after the Digne Nappe emplacement (Hippolyte and Dumont, 2000; Balansa et al., 2022). Despite different fold timing, this observation questions the structural style of the folds in this Tertiary Valensole basin.

6.3. Implications at large scale on the structural style

6.3.1 Model of basement deformation and basement thrust wedge

The late deformation of the Digne-Barles area can be induced by basement deformation inducing the structural culmination of the Barles fold and thrust belt and the folding of the Digne Nappe (Schwartz et al., 2017; Balansa et al., 2022). Few studies have focused on the involvement of the basement during the pre-nappe stage. It was recently proposed that the Digne basin can be interpreted as a triangle zone model (Balansa et al., 2022). In this model, the accumulation of Miocene deposits in the Velodrome and Thoard area could have blocked the forward thrust propagation and localized the deformation in a triangle zone. Balansa et al. (2022) suggest that the syn-sedimentary deformation located in the northern part of the Valensole indicates the activation of the Barles fold system. They propose that this folding system requires the activation of deep basement structures. This triangle zone will accumulate some deformation until a backward deformation develops. After the Digne Nappe event, the basement thrust wedge continues to develop with a transfer of the deformation at the front in

the basement, probably due to the lack of Triassic evaporites on the Valensole margin. This will then induce the folding of the Digne Nappe and uplift of the Barles half-window. Figure 23 shows the projection of our 3D geometrical model on the 2D cross-section proposed by Balansa et al. (2022). Although at first sight our model seems compatible with the overall cross-section and the deep structures, some incompatibilities can be observed. The m2 molasse growth strata of the northern part of the Velodrome are compatible with the activation of the Barles fold system, but the growth strata observed in the southern part are, in this model, only explained by a supposed back-thrust in the southern part. This back-thrust is indeed required to explain the northward reversal of the Miocene series. The activation of this back-thrust proposed by Balansa et al. (2022) (Fig.3 and 23) seems mainly post-m2 and thus explains neither the age of the growth strata (since m1-2) nor the amplitude of the wedge. Moreover, evidences for a such structure are weak (small fault on the geological map, small offset i.e Miocene on Miocene). We rather interpret the surface expression of this zone as the tight hinge of the Bès syncline combined with the m2 fanning strata (Fig 7). Moreover, we concluded above that the tight overturned NW verging Bès fold (Figs.3 and 7) prolongates westward under the Tanaron Formation and the Digne Nappe from Esclangon village to Lambert village, whereas the common interpretation tends to connect the Vélodrome beds with the Valensole ones under and south of La Robine unit (Goguel, 1939; Crumeyrolle et al., 1991; Gidon and Pairis, 1992; Gidon, 1997; Fournier et al., 2008; Balansa et al., 2022).

One way to explain the tight overturning of the Bès fold is to make the Aiguebelle Unit the result of a back-thrust over the Miocene series and underneath the Digne Nappe (Gidon and Paris, 1992) (Fig.3 and 23). In this case, the Bès fold could be considered as a drag fold formed underneath the north-verging back-thrust. However, the Vélodrome is a structure with overturned or even recumbent folds in its four extremities with the Esclangon fold in the east, the Auribeau fold in the north, the Bès fold in the south and the recumbent bed dipping to the west at the west of Lambert village that could indicate a NS-striking recumbent fold (Fig.5). This strong non-cylindrical structure seems hard to explain with a simple triangle zone model with back-thrusting.

6.3.2. Salt-tectonics hypothesis

Recent scientific developments in this region have suggested that, during the collision phase and before, evaporites and salt-controlled tectonics played an important role in the development

of the fold-and-thrust belt. Numerous inherited salt structures formed during the Early and Middle Jurassic rifting, phases were described as reactivated during the Alpine shortening starting in the late Cretaceous (Ehtechamzadeh Afchar and Gidon, 1974; Mascle et al., 1988; Dardeau and Graciansky, 1990; Dardeau et al., 1990, Célini et al., 2020a, 2021). In the area around the Barles half-window, many structures have been described as evidence of salt tectonics as early as the rifting phase, from early Liassic to middle Jurassic, forming reactive diapirs, walls and megaflap (Goguel, 1939; Graham et al., 2012; Célini et al., 2020a, b, 2021), In this area, the Alpine compression used the weakness of the salt diapirs, walls, and sheets to localize many tectonic structures (Graham et al., 2012; Célini et al., 2020a, 2021). Célini et al. (2022) proposed that the Vélodrome formed by subsidence into a salt glacier outcropping during the Oligocene time and making the Vélodrome a secondary mini-basin (Célini et al., 2022; Graham et al., 2012). Figure 23 shows the projection of our 3D geometrical model on the 2D cross-section proposed by Celini et al. (2022). The main difference with the cross-section of Balansa et al. (2022) is the thickening of the Nappe stack by doubling the Mesozoic series with thin-skin tectonics instead of invoking an early involvement of the basement. In this case, our modeling is also in accordance with the cross-section. The Celini et al. (2022) cross-section shows both in the southern and the northern part of the Velodrome some salt movements– features often observed in salt-related mini-basins (e.g. Giles and Rowan, 2012). As described above, the Vélodrome strata display successive unconformities, onlaps, and growth strata – since the Burdigalian layers in the north and since the Aquitanian in the south. The northern unconformities in the m2 can be explained by syn-tectonic, or salt escape as proposed by Celini et al. (2022).

By using the salt hypothesis a step further, and considering the isopach sequence of the Aquitanian-Burdigalian overturned beds, compared to the lower tilt of the underlying Mesozoic beds, we can hypothesize the formation of a megaflap (initially a carapace above the salt mass, later overturned during Middle-Late Burdigalian). As described before, the growth geometry near the southeastern termination of the Vélodrome is difficult to explain by the activation of a back-thrust and rather in accordance with growth sequences controlled by salt escape. In this case, the discontinuity between the Oligocene and Miocene series could not be a simple fault but rather a salt-related weld or a thrust weld (Celini et al., 2022). As explained above, the edges of the Velodrome correspond to either overturned or recumbent folds. This closed structure could be compatible with a mechanism of a bucket-like minibasin with internal unconformities

(Callot et al., 2016; Fernandez et al., 2017) that would be superimposed to the regional flexural subsidence as proposed by Celini et al. (2022).

This interpretation involving a significant component of salt-tectonics is however debatable. The salt-tectonics hypothesis of Graham et al. (2012) and Célini et al. (2022) involves salt walls derived from a canopy in the north and south that moved during the Oligocene as a thrust plug glacier (such as those described in the Betics, see Flinch and Soto (2022), which accommodated the Vélodrome enhanced local accommodation as a secondary minibasin. For the occurrence of a weld located north of the Vélodrome separating the Miocene beds from the underlying Mesozoic beds, no direct field evidences, nor clear discontinuity other than the basal unconformity of the Oligocene molasse have been observed. This does not necessarily preclude its existence, as concordant welds (expected for salt sheet) are generally poorly expressed (see Hudec and Jackson 2017; Kergaravat et al., 2017). Indeed, the presence of the thick breccia in the lower part of the Oligocene molasse, as well as the observation of slumps within the Molasse Rouge north of the abandoned Esclangon old village (Haccard et al., 1989a) could witness such a weld within Oligocene strata (Célini et al., 2022). For the existence of a salt-glacier in the south, which remains could be the chaotic and olistolithic Tanaron Formation, as postulated by Célini et al. (2021), is also a possibility. In this case, the salt-glacier could have also subsequently received olistoliths resulting from the erosion of the Barles fold and thrust belt and the Digne nappe. However, our approach does not provide any specific tests in this regard. Moreover, the presence farther west of salted marsh and sebkhas have been documented in the Oligocene beds close to Sorine with Sr Signature close to those of Triassic beds (Hamon, 2022).

To conclude with the salt-tectonics hypothesis, the 3D modelling approach described in the present paper confirms the non-cylindricity and the syn-sedimentation folding of the Vélodrome and its bucket-like shape, all characteristics often present in salt-related mini-basins. The salt hypothesis is also considered as one of the possible explanations consistent with the geometries observed in the Velodrome. Further studies are however necessary to further test this hypothesis, especially the existence of a salt canopy that cannot be tested by a simple geometrical approach.

7. Conclusion

This 3D geometrical modelling approach combined with detailed field data acquired by UAV photogrammetric data and on foot provides a thorough 3D overview of the tectono-sedimentary evolution of the foreland Vélodrome basin in front of the Digne Nappe thrust, the youngest and most external thrust in the southwestern Alps. This study brings new constrains on the Vélodrome internal geometries and highlights the 3D shape of the structure. The Vélodrome presents several folds with different orientations, mostly overturned strata in opposite directions, and synorogenic deposits with progressive unconformities. This new understanding of the inter- and intraformation geometries in the Vélodrome allows specifying the deformation sequence in the Digne Nappe area. Deformation started in the Aquitanian in the south and believed to be associated with salt-related tectonics, highlighted by abrupt unconformities and tightly overturned folding. In the north, the deformation only began during the Burdigalian, as shown by conformable Aquitanian and lower Burdigalian strata and the occurrence of growth strata in the middle and late Burdigalian. The modelled geometry allows us discussing the different published hypotheses for the formation of the Vélodrome the classical hypothesis due to a syn-sedimentary folding, which remains compatible with most of our data and models versus the mini-basin related to salt-tectonics hypothesis recently published, which is also compatible. This study shows that the 3D geometrical modelling approach with the Geomodeller is a powerful tool for testing different hypotheses and thus better understand 3D complex structures at the front of thrust belts such as the Vélodrome.

Supplementary materials

The supplementary materials consist of :

(1) Supplementary stratigraphic details on mio-pliocene molasse

(2) a 3D pdf presenting the final model of the Vélodrome, corresponding to the model testing the syn-deposit hypothesis

(2) the structural data used to realize the final model of the Vélodrome.

Supplementary stratigraphic details on mio-pliocene molasse

The age of marine and continental molasses found in Velodrome Mio-pliocene sediments (described in 2.2 and Fig.2.a) is still being debated.

The bird footprint-rich conglomeratic molasse is sometimes described as starting in Early Burdigalian, but outcrops described by Couëffé and Maridet (2003) indicate that the onset of marine conditions is rather middle Aquitanian (biozone MN 2a; Kälin, 1997; Kempf et al., 1997) followed by the marly and sandy molasse starting during the Early Burdigalian (occurrence of Burdigalian pectens (Haccard et al., 1989) and nannoflora Helicosphaera ampliaperta (Bramlette and Wilcoxon, 1967) indicating nannozones NN3 et NN4). The Cerithes-rich molasse is classically attributed to the Langhian-Tortonian (Haccard et al., 1989a) but this age has been revised by Coueffe and Maridet (2003) to Langhian based on biostratigraphic data (mammals attributed to biozone MN5 (Kälin 1997, Kempf et al., 1997)).

The age of the top of this molasse succession (also the top of the m4-p) is still unclear. From Gigot et al. (1974) and Haccard et al. (1989) the age of this residual basin corresponding to the deposits of the olistolithic Tanaron Formation is attributed to the Pliocene or late Pliocene by regional correlation, but without biostratigraphic data (see also Hippolyte et al. 2011 for a more detailed discussion). Hippolyte et al. (2011) have observed that the pre-messinian fluvial formation of the Valensole formation (Valensole-1) has been incised by a tributary of a paleo-Bléone, then infilled by the Tanaron formation. This would argue for a late-Messinian/early Pliocene age for the Tanaron Formation if we consider this erosional event linked to the Messinian event at regional scale (Hippolyte et al., 2011). Although not in the core of our work, the age of this formation is important for dating the advancement of the Digne nappe that overthrusted the Velodrome and the residual basin. Early papers (Gigot et al. 1974; Clauzon 1975; Haccard et al., 1989a) described a Miocene first emplacement of the Digne Nappe proceeding until the late Pliocene, followed by large-scale folding and formation of the Barles half-window. Gidon and Pairis (1988; 1992) argued instead that the nappe was already in the Digne area in the Late Miocene and continued to move afterward. The thermochronological study of Schwartz et al. (2017) tends to confirm this latter interpretation by suggesting a burial of 3-4 km underneath the Digne nappe by 6 Ma, which would prevent the deposition of a basin in the Pliocene. However, their samples were taken from the early Miocene and Oligocene not in contact with the residual basin, and they introduced *a priori* constraint boxes in their t-T inverse modeling, which does not give for an exhumation at 6 Ma. There thus remains space for discussion on the exact age of the most recent Valensole basin deposits between the Messinian and the Early Pliocene.

References

Ahmadhadi, F., Daniel, J.-M., Azzizadeh, M., Lacombe, O., 2008. Evidence for pre-folding vein development in the Oligo-Miocene Asmari Formation in the Central Zagros Fold Belt, Iran: FRACTURE PATTERNS WITHIN ASMARI FM, IRAN. Tectonics 27, n/a-n/a. https://doi.org/10.1029/2006TC001978

Andreani, L., Loget, N., Rangin, C., Le Pichon, X., 2010. New structural constraints on the southern Provence thrust belt (France): evidences for an Eocene shortening event linked to the

Corsica-Sardinia subduction. Bulletin de la Société Géologique de France 181, 547–563. https://doi.org/10.2113/gssgfbull.181.6.547

Antoine, P.-O., Stutz, N.S., Guiomar, M., 2022. Mesaceratherium gaimersheimense Heissig, 1969 (Mammalia, Rhinocerotidae) de La Javie (Oligocène supérieur, SE France). Presented at the Congrès Association Paléontologique Française (APF) 2022 : "Bicentenaire du mot Paléontologie," Montpellier, France.

Apps, G., Peel, F., Elliott, T., 2004. The structural setting and palaeogeographical evolution of the Grès d'Annot Basin. The Geological Society of London 221, 65–96.

Aubourg, C., Rochette, P., Stéphan, J.-F., Popoff, M., Chabert-Pelline, C., 1999. The magnetic fabric of weakly deformed Late Jurassic shales from the southern subalpines chains (French Alps): evidence for SW-directed tectonic transport direction. Tectonophysics 307, 15–31. https://doi.org/10.1016/S0040-1951(99)00116-X

Balansa, J., Espurt, N., Hippolyte, J.-C., Philip, J., Caritg, S., 2022. Structural evolution of the superimposed Provençal and Subalpine fold-thrust belts (SE France). Earth-Science Reviews 227, 103972. https://doi.org/10.1016/j.earscirev.2022.103972

Balestra, M., Corrado, S., Aldega, L., Rudkiewicz, J.-L., Gasparo Morticelli, M., Sulli, A., Sassi, W., 2019. 3D structural modeling and restoration of the Apennine-Maghrebian chain in Sicily: Application for non-cylindrical fold-and-thrust belts. Tectonophysics 761, 86–107. https://doi.org/10.1016/j.tecto.2019.04.014

Beck, C., Deville, E., Blanc, E., Philippe, Y., Tardy, M., 1998. Horizontal shortening control of Middle Miocene marine siliciclastic accumulation (Upper Marine Molasse) in the southern termination of the Savoy Molasse Basin (northwestern Alps/southern Jura). SP 134, 263–278. https://doi.org/10.1144/GSL.SP.1998.134.01.12

Bellahsen, N., Mouthereau, F., Boutoux, A., Bellanger, M., Lacombe, O., Jolivet, L., Rolland, Y., 2014. Collision kinematics in the western external Alps: Kinematics of the Alpine collision. Tectonics 33, 1055–1088. https://doi.org/10.1002/2013TC003453

Besson, D., Parize, O., Rubino, J.-L., Aguilar, J.-P., Aubry, M.-P., Beaudoin, B., Berggren, W.A., Clauzon, G., Crumeyrolle, P., Dexcoté, Y., Fiet, N., Iaccarino, S., Jiménez-Moreno, G., Laporte-Galaa, C., Michaux, J., Von Salis, K., Suc, J.-P., Reynaud, J.-Y., Wernli, R., 2005. Un réseau fluviatile d'âge Burdigalien terminal dans le Sud-Est de la France : remplissage, extension, âge, implications. Comptes Rendus Geoscience 337, 1045–1054. https://doi.org/10.1016/j.crte.2005.05.009

Bestani, L., Espurt, N., Lamarche, J., Floquet, M., Philip, J., Bellier, O., Hollender, F., 2015. Structural style and evolution of the Pyrenean-Provence thrust belt, SE France. Bulletin de la Société Géologique de France 186, 223–241. https://doi.org/10.2113/gssgfbull.186.4-5.223

Bialkowski, A., 2002. Stratigraphie isotopique (carbone et oxygène) des séries continentales d'un bassin d'avant-pays (Oligo-Miocène du bassin de Digne-Valensole) Paléoenvironnement et séquences de dépôts.

Bigot-Cormier, F., Poupeau, G., Sosson, M., 2000. Dénudations différentielles du massif cristallin externe alpin de l'Argentera (Sud-Est de la France) révélées par thermochronologie

traces de fission (apatites, zircons). Comptes Rendus de l'Académie des Sciences - Series IIA - Earth and Planetary Science 330, 363–370. https://doi.org/10.1016/S1251-8050(00)00127-0

Bistacchi, A., Massironi, M., Dal Piaz, G.V., Dal Piaz, G., Monopoli, B., Schiavo, A., Toffolon, G., 2008. 3D fold and fault reconstruction with an uncertainty model: An example from an Alpine tunnel case study. Computers & Geosciences 34, 351–372. https://doi.org/10.1016/j.cageo.2007.04.002

Bramlette, M.N., Wilcoxon, J.A., 1967. Middle Tertiary calcareous nannoplankton of the Cipero section, Trinidad, W. I. Tulane Studies in Geology 5, 93–131.

Brooke-Barnett, S., 2022. The effects of salt tectonics in the evolution of a fold and thrust belt, south-west Alps.

Buckley, S.J., Ringdal, K., Naumann, N., Dolva, B., Kurz, T.H., Howell, J.A., Dewez, T.J.B., 2019. LIME: Software for 3-D visualization, interpretation, and communication of virtual geoscience models. Geosphere 15, 222–235. https://doi.org/10.1130/GES02002.1

Burrel, L., Teixell, A., 2021. Contractional salt tectonics and role of pre-existing diapiric structures in the Southern Pyrenean foreland fold–thrust belt (Montsec and Serres Marginals). JGS 178, jgs2020-085. https://doi.org/10.1144/jgs2020-085

Calcagno, P., Chilès, J.P., Courrioux, G., Guillen, A., 2008. Geological modelling from field data and geological knowledge. Physics of the Earth and Planetary Interiors 171, 147–157. https://doi.org/10.1016/j.pepi.2008.06.013

Callot, J.P., Jahani, S., Letouzey, J., 2007. The Role of Pre-Existing Diapirs in Fold and Thrust Belt Development, in: Lacombe, O., Roure, F., Lavé, J., Vergés, J. (Eds.), Thrust Belts and Foreland Basins, Frontiers in Earth Sciences. Springer Berlin Heidelberg, Berlin, Heidelberg, pp. 309–325. https://doi.org/10.1007/978-3-540-69426-7_16

Callot, J.-P., Ribes, C., Kergaravat, C., Bonnel, C., Temiz, H., Poisson, A., Vrielynck, B., Salel, J.-F., Ringenbach, J.-C., 2014. Salt tectonics in the Sivas basin (Turkey): crossing salt walls and minibasins. Bulletin de la Société Géologique de France 185, 33–42. https://doi.org/10.2113/gssgfbull.185.1.33

Callot, J.-P., Salel, J.-F., Letouzey, J., Daniel, J.-M., Ringenbach, J.-C., 2016. Three-dimensional evolution of salt-controlled minibasins: Interactions, folding and megaflap development. Bulletin 100, 1419–1442. https://doi.org/10.1306/03101614087

Callot, J.-P., Trocmé, V., Letouzey, J., Albouy, E., Jahani, S., Sherkati, S., 2012. Pre-existing salt structures and the folding of the Zagros Mountains. Geological Society, London, Special Publications 363, 545–561. https://doi.org/10.1144/SP363.27

Célini, N., 2020. Le rôle des évaporites dans l'évolution tectonique du front alpin : cas de la nappe de Digne.

Célini, N., Callot, J., Ringenbach, J., Graham, R., 2020. Jurassic Salt Tectonics in the SW Sub-Alpine Fold-and-Thrust Belt. Tectonics 39. https://doi.org/10.1029/2020TC006107

Célini, N., Callot, J.-P., Pichat, A., Legeay, E., Graham, R., Ringenbach, J.-C., 2022. Secondary minibasins in orogens: Examples from the Sivas Basin (Turkey) and the sub-Alpine fold-and-thrust belt (France). Journal of Structural Geology 156, 104555. https://doi.org/10.1016/j.jsg.2022.104555

Célini, N., Callot, J.-P., Ringenbach, J.-C., Graham, R., 2021. Anatomy and evolution of the Astoin diapiric complex, sub-Alpine fold-and-thrust belt (France). BSGF - Earth Sci. Bull. 192, 29. https://doi.org/10.1051/bsgf/2021018

Célini, N., Mouthereau, F., Lahfid, A., Gout, C., Callot, J.-P., 2023. Rift thermal inheritance in the SW Alps (France): insights from RSCM thermometry and 1D thermal numerical modelling. Solid Earth 14, 1–16. https://doi.org/10.5194/se-14-1-2023

Clauzon, G., 1975. Sur l'âge villafranchien du chevauchement subalpin au droit de Puimoisson (Alpes-de-Haute-Provence). C. R. Acad. Sc. Paris 280, 2433–2436.

Collon, P., Pichat, A., Kergaravat, C., Botella, A., Caumon, G., Ringenbach, J.-C., Callot, J.-P., 2016. 3D modeling from outcrop data in a salt tectonic context: Example from the Inceyol minibasin, Sivas Basin, Turkey. Interpretation 4, SM17–SM31. https://doi.org/10.1190/INT-2015-0178.1

Cotillon, P., Gigot, P., Haccard, D., Monjuvent, G., 2013. Carte géol. de la France (1/50000). feuille SISTERON (917).

Couëffé, R., Maridet, O., 2003. Découverte de deux gisements à micromammifères du Burdigalien supérieur dans la Molasse Marine du bassin de Digne (Alpes de Haute-Provences, SE France) : implications stratigraphiques et tectoniques. https://doi.org/10.5169/SEALS-169015

Courtillot, V., Dagbert, M., Chermette, J.-C., Goguel, J., Guillemot, J., 1981. Carte géologique de la France à 1/50 000. 944, DIGNE.

Coward, M., Dietrich, D., 1989. Alpine tectonics — an overview. Geological Society, London, Special Publications 45, 1–29. https://doi.org/10.1144/GSL.SP.1989.045.01.01

Crumeyrolle, P., Rubino, J.-L., Clauzon, G., 1991. Miocene depositional sequences within a tectonically controlled transgressive-regressive cycle. Spec. Publs. int. Ass. Sediment 12, 373–390.

Dardeau, G., Fortwengler, D., Grasciansky, P.-C. de, Jacquin, T., Marchand, D., Martinod, J., 1990. Halocinèse et jeu de blocs dans les Baronnies : diapirs de Propriac, Montaulieu, Condorcet (département de la drôme, France). Bull. Centres Rech. Explor. - Prod. Elf-Aquitaine 14, 111–159.
Dardeau, G., Graciansky, P.-C.D., 1990. Halocinèse et rifting téthysien dans les Alpes-maritimes (France). Bull. Centres Rech. Explor. -Prod. Elf-Aquitaine 14, 443–464.
Davis, D.M., Engelder, T., 1985. The role of salt in fold-and-thrust belts. Tectonophysics 119, 67–88. https://doi.org/10.1016/0040-1951(85)90033-2

Decarlis, A., Maino, M., Dallagiovanna, G., Lualdi, A., Masini, E., Seno, S., Toscani, G., 2014. Salt tectonics in the SW Alps (Italy–France): From rifting to the inversion of the European

continental margin in a context of oblique convergence. Tectonophysics 636, 293–314. https://doi.org/10.1016/j.tecto.2014.09.003

DeCelles, P.G., 2012. Foreland Basin Systems Revisited: Variations in Response to Tectonic Settings, in: Busby, C., Azor, A. (Eds.), Tectonics of Sedimentary Basins. John Wiley & Sons, Ltd, Chichester, UK, pp. 405–426. https://doi.org/10.1002/9781444347166.ch20

Dubar, M., 1984. Chronologie et signification des dépôts continentaux du Néogène supérieur du bassin de Riez-Valensole (Alpes-de-Haute-Provence, France). Bull. Soc. géol. France XXVI, 971–978.

Dubar, M., Guérin, C., Heintz, E., 1978. Les nouveaux gisements villafranchiens du ravin de cornillet (moustiers sainte-marie, alpes de haute provence, france) et leur contexte géologique. Géobios 11, 367–381.

Duffy, O.B., Dooley, T.P., Hudec, M.R., Jackson, M.P.A., Fernandez, N., Jackson, C.A.-L., Soto, J.I., 2018. Structural evolution of salt-influenced fold-and-thrust belts: A synthesis and new insights from basins containing isolated salt diapirs. Journal of Structural Geology 114, 206–221. https://doi.org/10.1016/j.jsg.2018.06.024

Dumont, T., 1988. Late Triassic-Early Jurassic evolution of the Western Alps and of their European foreland; initiation of the Tethyan rifting. Bulletin de la Société Géologique de France IV, 601–611. https://doi.org/10.2113/gssgfbull.IV.4.601

Dumont, T., Schwartz, S., Guillot, S., Simon-Labric, T., Tricart, P., Jourdan, S., 2012. Structural and sedimentary records of the Oligocene revolution in the Western Alpine arc. Journal of Geodynamics 56–57, 18–38. https://doi.org/10.1016/j.jog.2011.11.006

Ehtechamzadeh Afchar, M., Gidon, M., 1974. Données nouvelles sur la structure de l'extrémité nord de la zone des chevauchements de Digne. Géologie Alpine 50, 57–69.

Fernandez, N., Duffy, O.B., Hudec, M.R., Jackson, M.P.A., Burg, G., Jackson, C.A.-L., Dooley, T.P., 2017. The origin of salt-encased sediment packages: Observations from the SE Precaspian Basin (Kazakhstan). Journal of Structural Geology 97, 237–256. https://doi.org/10.1016/j.jsg.2017.01.008

Flinch, J.F., Soto, J.I., 2022. Structure and Alpine tectonic evolution of a salt canopy in the western Betic Cordillera (Spain). Marine and Petroleum Geology 143, 105782. https://doi.org/10.1016/j.marpetgeo.2022.105782

Ford, Lickorish, Kusznir, 1999. Tertiary foreland sedimentation in the Southern Subalpine Chains, SE France: a geodynamic appraisal: Sedimentation in the Southern Subalpine Chains. Basin Research 11, 315–336. https://doi.org/10.1046/j.1365-2117.1999.00103.x
Ford, M., Duchêne, S., Gasquet, D., Vanderhaeghe, O., 2006. Two-phase orogenic convergence in the external and internal SW Alps. Journal of the Geological Society 163, 815–826. https://doi.org/10.1144/0016-76492005-034

Ford, M., Lickorish, W.H., 2004. Foreland basin evolution around the western Alpine Arc. The Geological Society of London 221, 39–63.

Fournier, M., Agard, P., Petit, C., 2008. Micro-tectonic constraints on the evolution of the Barles half-window (Digne nappe, southern Alps). Implications for the timing of folding in the Valensole foreland basin. Bulletin de la Société Géologique de France 179, 551–568. https://doi.org/10.2113/gssgfbull.179.6.551

Frank, T., Tertois, A.-L., Mallet, J.-L., 2007. 3D-reconstruction of complex geological interfaces from irregularly distributed and noisy point data. Computers & Geosciences 33, 932–943. https://doi.org/10.1016/j.cageo.2006.11.014

Ghosh, S.K., Deb, S.K., Sengupta, S., 1996. Hinge migration and hinge replacement. Tectonophysics 263, 319–337. https://doi.org/10.1016/S0040-1951(96)00031-5

Gidon, M., 1997. Les chaînons subalpins au nord-est de Sisteron et l'histoire tectonique de la nappe de Digne. Géologie Alpine 73, 23–57.

Gidon, M., Monjuvent, G., Flandrin, J., Moullade, M., Durozoy, G., Damiani, L., 1991. Carte géologique de la France à 1/50 000. 893, Laragne-Montéglin.

Gidon, M., Pairis, J.-L., 1992. Relations entre le charriage de la Nappe de Digne et la structure de son autochtone dans la vallée du Bès (Alpes de Haute Provence, France). Eclogae geol. Helv. 85, 327–359.

Gidon, M., Pairis, J.-L., 1988. La structure des environs de Digne (Chaînes subalpines méridionales, Alpes-de-Haute-Provence) : un exemple d'interférence entre l'avancée d'une nappe de charriage épiglyptique et la sédimentation sur son front. C.R. Acad. Sc. Paris 1283–1288.

Gidon, M., Pairis, J.-L., 1986. La nappe de Digne (Chaînes subalpines méridionales) : origine, déplacement et signification régionale. C.R. Acad. Sc. Paris 981–984.

Gigot, P., Grandjacquet, C., Haccard, D., 1974. Evolution tectono-sédimentaire de la bordure septentrionale du bassin tertiaire de Digne depuis l'Eocène. B.S.G.F 7, 128–139.

Gigot, P., Thomel, G., Colomb, E., Dubar, M., Durozoy, G., Damiani, L., 1982. Notice explicative, carte géol. France (1/50 000), feuille FORCAQUIER (943) - Orléans : Bureau de recherches géologiques et minières, 27 p. Carte géologique par Gigot, P., Thomel, G., Colomb, E., Dubar, M., Durozoy, G., Damiani, L. (1982).

Giles, K.A., Rowan, M.G., 2012. Concepts in halokinetic-sequence deformation and stratigraphy. Geological Society, London, Special Publications 363, 7–31. https://doi.org/10.1144/SP363.2

Goguel, J., 1963. L'interpretation de l'arc des Alpes occidentales. Bulletin de la Société Géologique de France S7-V, 20–33. https://doi.org/10.2113/gssgfbull.S7-V.1.20

Goguel, J., 1939. Tectonique des chaines subalpines entre la Bléone et la Durance- Alpes 40.

Graciansky, P.C., Dardeau, G., Lemoine, M., Tricart, P., 1989. The inverted margin of the French Alps and foreland basin inversion. Geological Society, London, Special Publications 44, 87–104. https://doi.org/10.1144/GSL.SP.1989.044.01.06

Graciansky, P.-C.D., Dardeau, G., Lemoine, M., Tricart, P., 1988. De la distension à la compression : l'inversion structurale dans les Alpes. Bull. Soc. géol. France 8, 779–785.

Graham, R., Jackson, M., Pilcher, R., Kilsdonk, B., 2012. Allochthonous salt in the sub-Alpine fold–thrust belt of Haute Provence, France. Geological Society, London, Special Publications 363, 595–615. https://doi.org/10.1144/SP363.30

Granado, P., Roca, E., Strauss, P., Pelz, K., Muñoz, J.A., 2019. Structural styles in fold-and-thrust belts involving early salt structures: The Northern Calcareous Alps (Austria). Geology 47, 51–54. https://doi.org/10.1130/G45281.1

Haccard, D., Beaudoin, B., Gigot, P., Jorda, M., 1989a. Notice explicative, carte géol. France (1/50 000), feuille LA JAVIE (918) - Orléans : Bureau de recherches géologiques et minières, 152 p. Carte géologique par Haccard D., Beaudoin B., Gigot P., Jorda M., et al. (1989).

Haccard, D., Beaudoin, B., Gigot, P., Jorda, M., et al., 1989b. Carte géol. de la France (1/50000). feuille LA JAVIE (918) - Orléans : Bureau de recherches géologiques et minières. Notice explicative par Haccard D., Beaudoin B., Gigot P., Jorda M., (1989), 152p.

Hamon, A., 2022. Les facteurs de contrôle de la sédimentation Éocène continentale dans les Alpes du Sud-Ouest à la limite Eocène-Oligocène. Ecole des mines de Fontainebleau.

Hippolyte, J.-C., Clauzon, G., Suc, J.-P., 2011. Messinian-Zanclean canyons in the Digne nappe (southwestern Alps): tectonic implications. Bulletin de la Société Géologique de France 182, 111–132. https://doi.org/10.2113/gssgfbull.182.2.111

Hippolyte, J.-C., Dumont, T., 2000. Identification of Quaternary thrusts, folds and faults in a low seismicity area: examples in the Southern Alps (France). Terra Nova 12, 156–162. https://doi.org/10.1046/j.1365-3121.2000.00287.x

Jackson, M.P.A., Hudec, M.R., 2017. Salt tectonics : Principles and Practice. Cambridge Univ. Press.

Jackson, M.P.A., Vendeville, B.C., 1994. Regional extension as a geologic trigger for diapirism. Geological Society of America Bulletin 106, 57–73. https://doi.org/10.1130/0016-7606(1994)106<0057:REAAGT>2.3.CO;2

Jorda, M., Combes, P., Philip, H., 1992. Tectogénèse et morphogénèse quaternaires des chaînes subalpines méridionales (région de Digne et vallée de la Bléone). quate 3, 129–135. https://doi.org/10.3406/quate.1992.1982

Jourdon, A., Mouthereau, F., Le Pourhiet, L., Callot, J., 2020. Topographic and Tectonic Evolution of Mountain Belts Controlled by Salt Thickness and Rift Architecture. Tectonics 39. https://doi.org/10.1029/2019TC005903

Kalifi, A., Leloup, P.H., Sorrel, P., Galy, A., Demory, F., Spina, V., Huet, B., Quillévéré, F., Ricciardi, F., Michoux, D., Lecacheur, K., Grime, R., Pittet, B., Rubino, J.-L., 2021. Chronology of thrust propagation from an updated tectono-sedimentary framework of the Miocene molasse (western Alps). Solid Earth 12, 2735–2771. https://doi.org/10.5194/se-12-2735-2021

Kalifi, A., Sorrel, P., Leloup, P.-H., Galy, A., Spina, V., Huet, B., Russo, S., Pittet, B., Rubino, J.-L., 2022. Tectonic control on the palaeogeographical evolution of the Miocene Seaway along the Western Alpine foreland basin. SP 523, 453–486. https://doi.org/10.1144/SP523-2021-78

Kälin, D., 1997. The mammal zonation of the Upper Marine Molasse of Switzerland reconsidered: A local biozonation of MN 2-MN 5. Mémoires et travaux de l'Institut de Montpellier 515–535.

Kempf, O., Bollinger, T., Kälin, D., Engesser, B., Matter, A., 1997. New magnetostratigraphic calibration of Early to Middle Miocene mammal biozones of the North Alpine foreland basin. Mémoires et travaux de l'Institut de Montpellier 547–561.

Kerckhove, C., 1969. La "zone du Flysh" dans les nappes de l'Embrunais-Ubaye (Alpes occidentales), Géologie Alpine.

Kergaravat, C., Ribes, C., Legeay, E., Callot, J.-P., Sevki Kavak, K., Ringenbach, J.-C., 2016. Minibasins and salt canopy in foreland fold-and-and-thrust belts : The central Sivas Basin, Turkey. Tectonics 35, 1342–1366. https://doi.org/10.1002/2016TC004186

Lacombe, O., Jolivet, L., 2005. Tectonics - 2005 - Lacombe - Structural and kinematic relationships between Corsica and the Pyrenees-Provence domain at the.pdf. Tectonics 24. https://doi.org/10.1029/2004TC001673

Lajaunie, C., Courrioux, G., Manuel, L., 1997. Foliation fields and 3D cartography in geology: Principles of a method based on potential interpolation. Math Geol 29, 571–584. https://doi.org/10.1007/BF02775087

Laurent, G., Ailleres, L., Grose, L., Caumon, G., Jessell, M., Armit, R., 2016. Implicit modeling of folds and overprinting deformation. Earth and Planetary Science Letters 456, 26–38. https://doi.org/10.1016/j.epsl.2016.09.040

Leeder, M.R., 2011. Tectonic sedimentology: sediment systems deciphering global to local tectonics: Tectonic sedimentology. Sedimentology 58, 2–56. https://doi.org/10.1111/j.1365-3091.2010.01207.x

Legeay, E., Ringenbach, J.-C., Kergaravat, C., Pichat, A., Mohn, G., Vergés, J., Kavak, K.S., Callot, J.-P., 2019. Structure and kinematics of the Central Sivas Basin (Turkey): salt deposition and tectonics in an evolving fold-and-thrust belt. Geological Society, London, Special Publications 490, 361–396. https://doi.org/10.1144/SP490-2019-92

Lemoine, M., 1972. Rythme et modalités des plissements superposés dans les Chaînes subalpines méridionales des Alpes occidentales françaises. Geol. Runsch. 61, 975–1010.

Lemoine, M., Bas, T., Arnaud-Vanneau, A., Arnaud, H., Dumont, T., Gidon, M., Bourbon, M., de Graciansky, P.-C., Rudkiewicz, J.-L., Megard-Galli, J., Tricart, P., 1986. The continental margin of the Mesozoic Tethys in the Western Alps. Marine and Petroleum Geology 3, 179–199. https://doi.org/10.1016/0264-8172(86)90044-9

Lickorish, W.H., Ford, M., 1998. Sequential restoration of the external Alpine Digne thrust system, SE France, constrained by kinematic data and synorogenic sediments. Geological Society, London, Special Publications 134, 189–211. https://doi.org/10.1144/GSL.SP.1998.134.01.09

Marroni, M., Feroni, A.C., di Biase, D., Ottria, G., Pandolfi, L., Taini, A., 2002. Polyphase folding at upper structural levels in the Borbera Valley (northern Apennines, Italy): implications for the tectonic evolution of the linkage area between Alps and Apennines. Comptes Rendus Geoscience 334, 565–572. https://doi.org/10.1016/S1631-0713(02)01784-4

Mascle, G., Arnaud, H., Dardeau, G., Debelmas, J., Delpech, P.-Y., Dubois, P., Gidon, M., Grasciansky, P.-C. de, Kerckhove, C., Lemoine, M., 1988. Salt tectonics, Tethyan rifting and Alpine folding in the French Alps. Bull. Soc. géol. France 8, 747–758.

Nabavi, S.T., Fossen, H., 2021. Fold geometry and folding – a review. Earth-Science Reviews 222, 103812. https://doi.org/10.1016/j.earscirev.2021.103812

Pairis, J.L., Gidon, M., 1987. Le détritisme Néogène et ses relations avec la tectonique à l'extrémité Nord-Est du Bassin de Valensole (Alpes externes méridionales). Géologie Alpine 417–426.

Pfiffner, O.A., 2014. Geology of the Alps 389.

Platt, J.P., 1986. Dynamics of orogenic wedges and the uplift of high-pressure metamorphic rocks. Geol Soc America Bull 97, 1037. https://doi.org/10.1130/0016-7606(1986)97<1037:DOOWAT>2.0.CO;2

Ramsay, J.G., 1962. Interference Patterns Produced by the Superposition of Folds of Similar Type. The Journal of Geology 70, 466–481. https://doi.org/10.1086/626837

Ribes, C., Kergaravat, C., Bonnel, C., Crumeyrolle, P., Callot, J.-P., Poisson, A., Haluk, T., Ringenbach, J.-C., 2015. Fluvial sedimentation in a salt-controlled mini-basin: stratal patterns and facies assemblages, Sivas Basin, Turkey. Sedimentology 62, 1513–1545. https://doi.org/10.1111/sed.12195

Rodrigues, R.T., Alkmim, F.F. de, Reis, H.L.S., Piatti, B.G., 2021. The role of tectonic inheritance in the development of a fold-thrust belt and superimposed rift: An example from the São Francisco basin, eastern Brazil. Tectonophysics 815, 228979. https://doi.org/10.1016/j.tecto.2021.228979

Rousset, C., Kerckhove, C., Bambier, A., 1983. Carte géol. de la France (1/50000). feuille SEYNE (894).

Saspiturry, N., Allanic, C., Serrano, O., Courrioux, G., Baudin, T., Le Bayon, B., Lahfid, A., Razin, P., Villasenor, A., Chevrot, S., Issautier, B., 2022. Upper lithospheric transfer zones driving the non-cylindricity of the West-Pyrenean orogenic prism (Mauléon hyperextended basin). Journal of Structural Geology 156, 104535. https://doi.org/10.1016/j.jsg.2022.104535

Schwartz, S., Gautheron, C., Audin, L., Dumont, T., Nomade, J., Barbarand, J., Pinna-Jamme, R., van der Beek, P., 2017. Foreland exhumation controlled by crustal thickening in the Western Alps. Geology 45, 139–142. https://doi.org/10.1130/G38561.1

Scrocca, D., 2006. Thrust front segmentation induced by differential slab retreat in the Apennines (Italy). Terra Nova 18, 154–161. https://doi.org/10.1111/j.1365-3121.2006.00675.x

Siddans, A.W.B., 1979. Acurate fold and thrust patterns in the Subalpine Chains of Southeast France. Journal of Structural Geology 1, 117–126.

Tavani, S., Storti, F., Lacombe, O., Corradetti, A., Muñoz, J.A., Mazzoli, S., 2015. A review of deformation pattern templates in foreland basin systems and fold-and-thrust belts: Implications for the state of stress in the frontal regions of thrust wedges. Earth-Science Reviews 141, 82–104. https://doi.org/10.1016/j.earscirev.2014.11.013

Thomel, G., Mercier, H., Gigot, P., 1982. Carte géologique de la France à 1/50 000. 943, Forcalquier.

Tricart, P., 1984. From passive margin to continental collision : a tectonic scenario for the western alps. American Journal of Science 284, 97–120.

Vignaroli, G., Faccenna, C., Rossetti, F., 2009. Retrogressive fabric development during exhumation of the Voltri Massif (Ligurian Alps, Italy): arguments for an extensional origin and implications for the Alps–Apennines linkage. Int J Earth Sci (Geol Rundsch) 98, 1077–1093. https://doi.org/10.1007/s00531-008-0305-4

Westoby, M.J., Brasington, J., Glasser, N.F., Hambrey, M.J., Reynolds, J.M., 2012. 'Structure-from-Motion' photogrammetry: A low-cost, effective tool for geoscience applications. Geomorphology 179, 300–314. https://doi.org/10.1016/j.geomorph.2012.08.021

Zulauf, G., Zulauf, J., Maul, H., 2017. Quantification of the geometrical parameters of non-cylindrical folds. Journal of Structural Geology 100, 120–129. https://doi.org/10.1016/j.jsg.2017.06.001

Figure table

Figure 1 : (a) Synthetic structural map of southwestern Alps, (b) Geological map of the Vélodrome area, modified from Haccard et al. (1989b), Gigot et al. (2013), Gidon et al. (1991), Rousset et al. (1983) . See Fig.1a for location of the map.

Figure 2 : (a) Synthetic log of the studied area (b) Surface NNE-SSW cross -section of the Barles area. See Fig.1 for location of the section .

Figure 3 : Interpreted panoramic view of the Velodrome from the south illustrating the bowl shape of the structure with overturned strata in different directions and the super-imposed Martellet anticline. Note that the southeast contact between the Oligocene and the chaotic facies of the top of the m4-p is unclear because the outcrops conditions do not allow to distinguish the autochtonous to the allochtonous bedding of the Molasse Rouge. Numbers in brackets correspond the heights of the main peaks. M.R. : Molasse Rouge; Val. Form. : Valensole Formation. The red dashes in the south correspond to faults or back-thrusts not observed in the

field but suggested by Haccard et al. (1989) and Gidon and Pairis (1992) to the north and the south respectively. Location of the Fig.7d, 8, 9, 10 and 20 are also indicated on this picture. See Fig.2 for formation references letters.

Figure 4 : Geological pile construction principle and the different possible relationships between series. Schemas illustrating three results of modelling in map view for the same data set with three different geological piles. Colored dots correspond to waypoints of the top of the corresponding formations.

Figure 5 : Geological map of the Vélodrome modified from Haccard et al. (1989). See Fig.1 for location and legend. Grey boxes present orientation mean values of each corresponding area. rev. = reversed. Black orientation symbols are field data, red orientation symbols are taken on 3D outcrops models obtained from drone picture.

Figure 6 : Series of cross-sections into the Vélodrome area illustrating its complex 3D structure. See Fig.5 for location of the sections. See Fig.1 for color legend.

Figure 7: View of the internal geometries and associated measurements in the southern and eastern parts of the Vélodrome. Uninterpreted (a) and interpreted (b) top view (toward the south) of eastern part of the Velodrome illustrating the superimposed Martellet anticline in the core of the structure. Uninterpreted (c) and interpreted (d) top view (toward the southwest) of the south-east termination of the Velodrome illustrating the tight overturned Bès syncline and the rapid unconformities of this area both in the m1-2 (Aquitanian- molasse) and m2 (Burdigalian molasse) units. The white line corresponds to the fold axis and the numbers to the average dip of each zone. Tanaron Fm. : Tanaron Formation; Jr: Jurassique; Tr: Trias; Ol: Oligocene. Pictures are extracted from a 3-D model obtained from stereoscopic aerial image (Source IGN, Photothèque Nationale, 05-09-1973). See Fig.3 and 7b for location. (e) Dip profil along cross section in the m2 (Burdigalian molasse) unit reported in Fig.7f. n is the number of presented data. (f) 3D model obtained from drone pictures and measurements realized directly on it with LIME software (Buckley et al., 2019) in the m2 (Burdigalian molasse). See Fig.7d for location. Yellow places represent the extension of planes measured on 3D model.

Figure 8 : Uninterpreted (a) and interpreted (b) picture of La Fubi area illustrating the recumbent fold of the m2(Burdigalian molasse)located in La Fubi unconformably lying on the uppest part of the Velodrome recumbent fold in the red marls of the Valensole Formation. See location of the picture on Fig.3 and view point on Fig.5.

Figure 9 : Uninterpreted (a) and interpreted (b) picture of La Fubi and La Coustagne outcrops illustrating the thrusting of both the folded Tithonian bloc and the folded m2 (Burdigalian molasse)on the Velodrome recumbent fold. See location of the picture on Fig.3 and viewpoint on Fig.5.

Figure 10 : (a) Picture of the hinge of the Auribeau syncline taken in the Valensole Formation in front of the Lame de Facibelle and the stereodiagram characterizing it. See Fig.3 and 10d for location. (b) Picture of the hinge of the Esclangon syncline taken in m1-2 (Aquitanian-Burdigalian molasse) and the stereodiagram characterizing it. See Fig. 3 and 17 for location. (c) Table characterizing axial surface and fold axis orientations of both folds. In the stereodiagram, grey lines correspond to the S0 of the folded strata, black dotted lines to the axial surface planes and red dot to the fold axis. (d) Drone view of the Auribeau syncline core. See Fig.5 for viewpoint location.

Figure 11 : Stereodiagram analyses characterizing the east (Esclangon crest, Z2 and Z3) and southeast (Bès fold Z1) area of the Vélodrome. White bedding symbols on the map correspond to the unused measurements for the stereodiagram analyses. The back-tilting has been realized in order to make the base of the nappe horizontal in the south. The orientation of the nappe considered is N077-47S.

Figure 12 : Details of internal geometries in Miocene units of the Vélodrome. (a), (b), (c) and (d) Dip profils along cross section in the lower Miocene formation. Sections are reported in (e) and (f) and in Fig.5. Red dot line in (a), (b) and (d) correspond to the mean dip of the strata. n is the number of presented data. (e) and (f) Picture of part of the Velodrome where detailed dip profils have been acquired. The blue and purple lines correspond the profiles. Orientation indications are the orientations of the mean surfaces. rev. : reversed

Figure 13 : Models of the Vélodrome, views from the ENE. Surfaces are the bottom surfaces of the formations. D.n. : Digne Nappe

Figure 14 : Input data and constraints imposed in the model (a) Map view of input data and working sections (b) Box model view from above with reference sections (c) Reference sections with interpretative constraints.

Figure 15 : EW-oriented cross-sections extracted from 3D models testing the post-deposit tectonic hypothesis (a) and the syn-deposit tectonic hypothesis (b). Location of the section is in the small map extracted from 3D models under right (black line). T.u. : Tanaron unit

Figure 16 : NNE/SSW-oriented cross-sections extracted from 3D models testing the post-deposit tectonic hypothesis (a) and the syn-deposit tectonic hypothesis (b). Location of the section is in the small map extracted from 3D models (black line). Note the difference of the upper limb geometries in the two hypotheses (upper limb highlighted by dashed lines in the section 2). See Fig.15 for legend.

Figure 17 : Views of the 3D models of the syn-deposit tectonic hypothesis. Surfaces correspond to the bottom surfaces of the formations. (a) Geological map extracted from the 3D model drapped on the MNT compared to the field panoramic view. (b) Zoom on the Bès fold showing its tightness and internal unconformities on Burdigalian to late Pliocene layers. (c) Zoom on the Coustagne area highlighting unconformities in the Miocene formations.

Figure 18 : Views of the modelled formation bottom surfaces for the syn-deposit tectonic hypothesis highlighting the cylindrical feature of the central and western part of the Vélodrome structure.

Figure 19 : Views of the 3D model of the southeast area of the Vélodrome computed only with map data. a) Section and map extracted from the model b) Map data used for this detailed model c) 3D views of the model showing the Bès fold.

Figure 20 : Two different views of the m1-2 (Aquitanian-Burdigalian molasse) of the Esclangon area illustrating the conformable feature of the molasse strata and the importance of the viewpoint location in 3D complex structures. See Fig.3 for location.

Fig 21 : Evidence of unconformities in the north of the Vélodrome and in the Mélan-Auribeau fold (a) Conceptual model of an isopaque fold (drawing in black) on which Vélodrome m2 (Burdigalian molasse) data have been projected (drawing in blue). Green line: section on which measures have been done. Numbers in black: dips corresponding to the isopaque conceptual

model of the fold. Numbers in blue: mean dips measured in the field. The arrows correspond to the dip variation along the section for the conceptual isopaque model in black and the field data in blue. n: normal bedding. r: reversed bedding. (b) Detailed geological map of the Mélan-Auribeau fold located west of the Vélodrome modified from Haccard et al.(1989). Red traces correspond to the interpretation of the satellite images (Google Earth, 2004 image) showing unconformities in the m2 (Burdigalian molasse) similar to that of Crumeyrolle et al. (1991) (Fig.5). Striped polygon corresponds to a chaotic zone that could be considered as a Tanaron equivalent formation.

Figure 22 : Synthetic tectonic map of the Velodrome area based of the Velodrome geological map (Fig.5) presenting a compilation of both observations confirmed by modelling and suggestion by the modelling See Fig.1 for location of the map.

Figure 23 : Projection of the Velodrome geometries extracted from the model into the two end-members large scale models from the literature. (a) Basement thrust wedge model, modified from Balansa et al. (2022). HF: Fault proposed by Haccard et al. (2022) and also adopted by Balansa et al. (2022). GPBT: Back-thrust between the oligocene and the Miocene formations proposed by Gidon and Pairis (1992); (b) Salt tectonics model, modified from Celini et al. (2022).

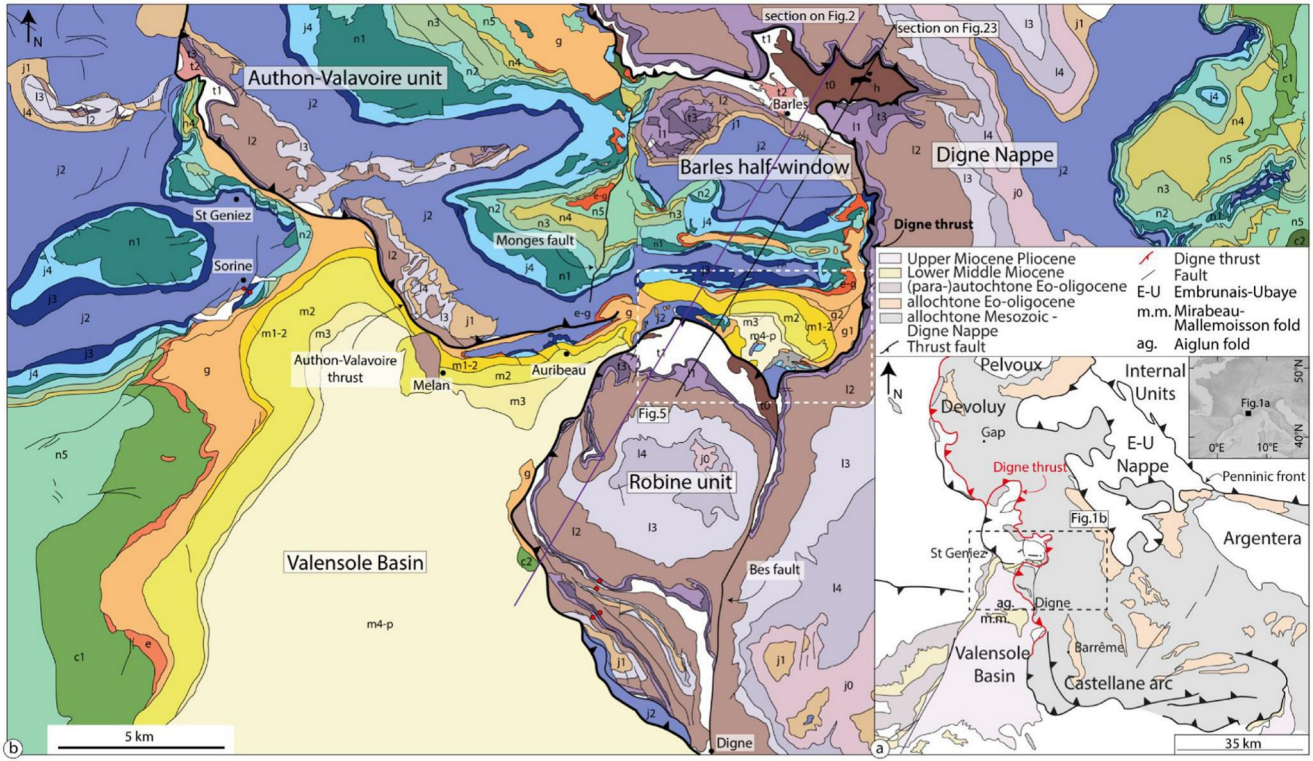
Authon-Valavoire unit
Barles half-window
Digne Nappe
Digne thrust
Monges fault
Authon-Valavoire thrust
Robine unit
Valensole Basin
Bes fault
St Geniez
Sorine
Melan
Auribeau
Barles
Digne
Fig.5
section on Fig.2
section on Fig.23
5 km
b
a
Upper Miocene Pliocene
Lower Middle Miocene
(para-)autochtone Eo-oligocene
allochtone Eo-oligocene
allochtone Mesozoic - Digne Nappe
Thrust fault
Digne thrust
Fault
E-U Embrunais-Ubaye
m.m. Mirabeau-Mallemoisson fold
ag. Aiglun fold
Pelvoux
Internal Units
Devoluy
Gap
E-U Nappe
Digne thrust
Penninic front
Fig.1b
Argentera
St Geniez
ag.
Digne
m.m.
Barrême
Valensole Basin
Castellane arc
Fig.1a
50°N
40°N
0°E
10°E
35 km
Tanaron Formation (T)
Upper Miocene - Pliocene (m4-p)
Langhian (m3)
Burdigalian (m2)
Aquitanian - Burdigalian (m1-2)
Lacustrine Oligocene (g2)
Continental Oligocene (g1)
undiff. Oligocene (g)
Eocene - Oligocene breccia (e-g)
undiff. Eocene (e)
Coniacian - Santonian (c2)
Cenomanian - Turonian (c1)
Aptian - Abian (n5)
Barremian (n4)
Hauterivian (n3)
Valanginian (n2)
Berriasian (n1)
Kimmeridgian - Tithonian (j4)
Middle - Upper Oxfordian (j3)
Bathonian - Callovian - Lower Oxfordian (j2)
Bajocian (j1)
Aalenian (j0)
Toarcian (l4)
Domerian (l3)
Sinemurian - Carixian (l2)
Hettangian (l1)
Rhaetian (t3)
Upper Triassic (t2)
Upper Triassic gypsum (t1)
Lower Middle Triassic (t0)
Stephanian basement (h)
Major faults and thrusts
Secondary faults
Normal stratification
Overturned stratification
Salt weld

Figure 1

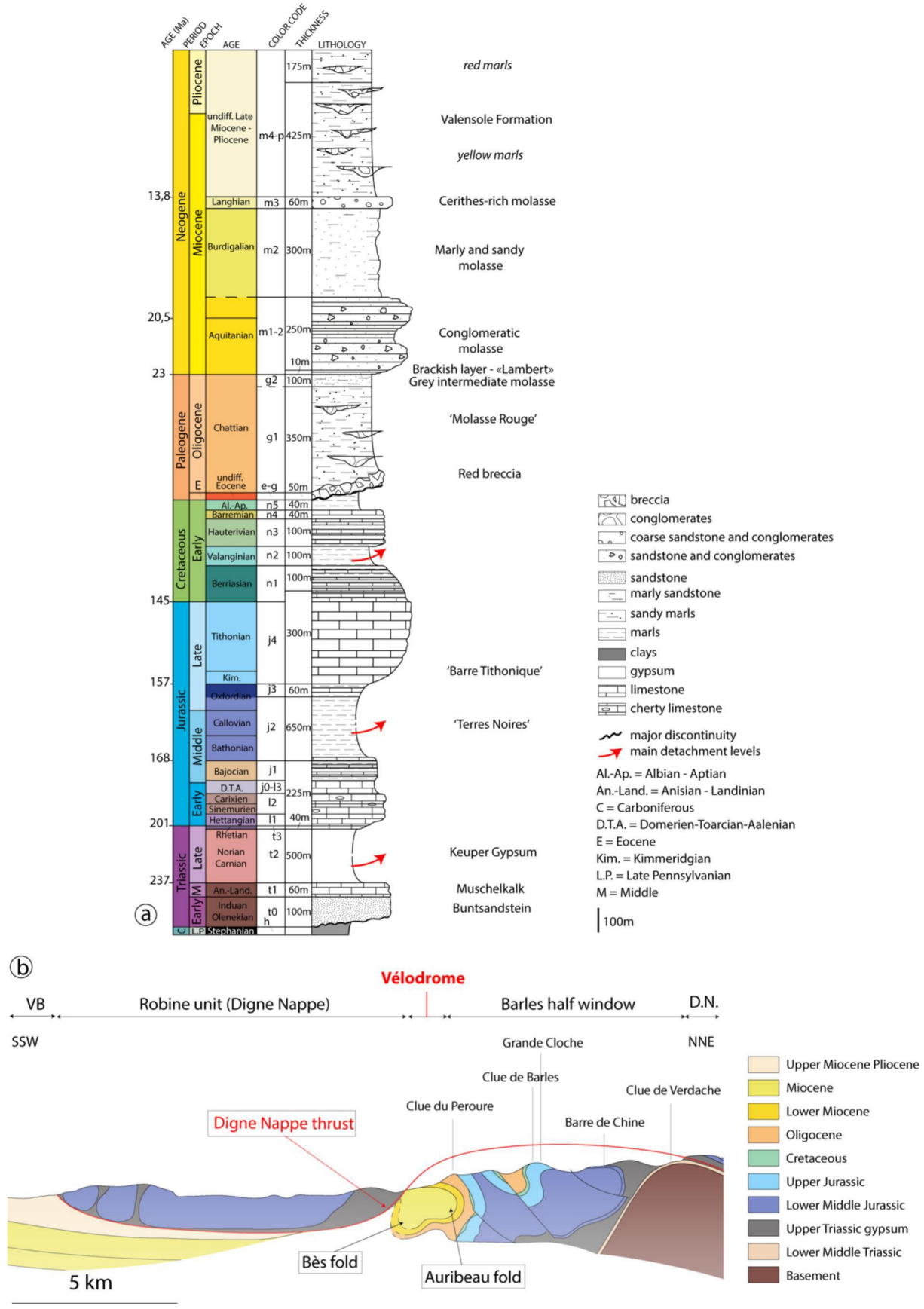
AGE (Ma)
PERIOD
EPOCH
AGE
COLOR CODE
THICKNESS
LITHOLOGY
Neogene
Pliocene
Miocene
Paleogene
Oligocene
Cretaceous
Early
Jurassic
Late
Middle
Early
Triassic
Late
Early
M
13,8
20,5
23
145
157
168
201
237
undiff. Late Miocene - Pliocene
Langhian
Burdigalian
Aquitanian
Chattian
undiff. Eocene
Al.-Ap.
Barremian
Hauterivian
Valanginian
Berriasian
Tithonian
Kim.
Oxfordian
Callovian
Bathonian
Bajocian
D.T.A.
Carixien
Sinemurien
Hettangian
Rhetian
Norian
Carnian
An.-Land.
Induan
Olenekian
Stephanian
m4-p
m3
m2
m1-2
g2
g1
e-g
n5
n4
n3
n2
n1
j4
j3
j2
j1
j0-l3
l2
l1
t3
t2
t1
t0
h
175m
425m
60m
300m
250m
10m
100m
350m
50m
40m
100m
300m
60m
650m
225m
40m
500m
60m
100m
red marls
Valensole Formation
yellow marls
Cerithes-rich molasse
Marly and sandy molasse
Conglomeratic molasse
Brackish layer - «Lambert»
Grey intermediate molasse
'Molasse Rouge'
Red breccia
'Barre Tithonique'
'Terres Noires'
Keuper Gypsum
Muschelkalk
Buntsandstein
a
breccia
conglomerates
coarse sandstone and conglomerates
sandstone and conglomerates
sandstone
marly sandstone
sandy marls
marls
clays
gypsum
limestone
cherty limestone
major discontinuity
main detachment levels
Al.-Ap. = Albian - Aptian
An.-Land. = Anisian - Landinian
C = Carboniferous
D.T.A. = Domerien-Toarcian-Aalenian
E = Eocene
Kim. = Kimmeridgian
L.P. = Late Pennsylvanian
M = Middle
100m
b
Vélodrome
VB
Robine unit (Digne Nappe)
Barles half window
D.N.
SSW
NNE
Grande Cloche
Clue de Barles
Clue de Verdache
Clue du Peroure
Barre de Chine
Digne Nappe thrust
Bès fold
Auribeau fold
5 km
Upper Miocene Pliocene
Miocene
Lower Miocene
Oligocene
Cretaceous
Upper Jurassic
Lower Middle Jurassic
Upper Triassic gypsum
Lower Middle Triassic
Basement

Figure 2

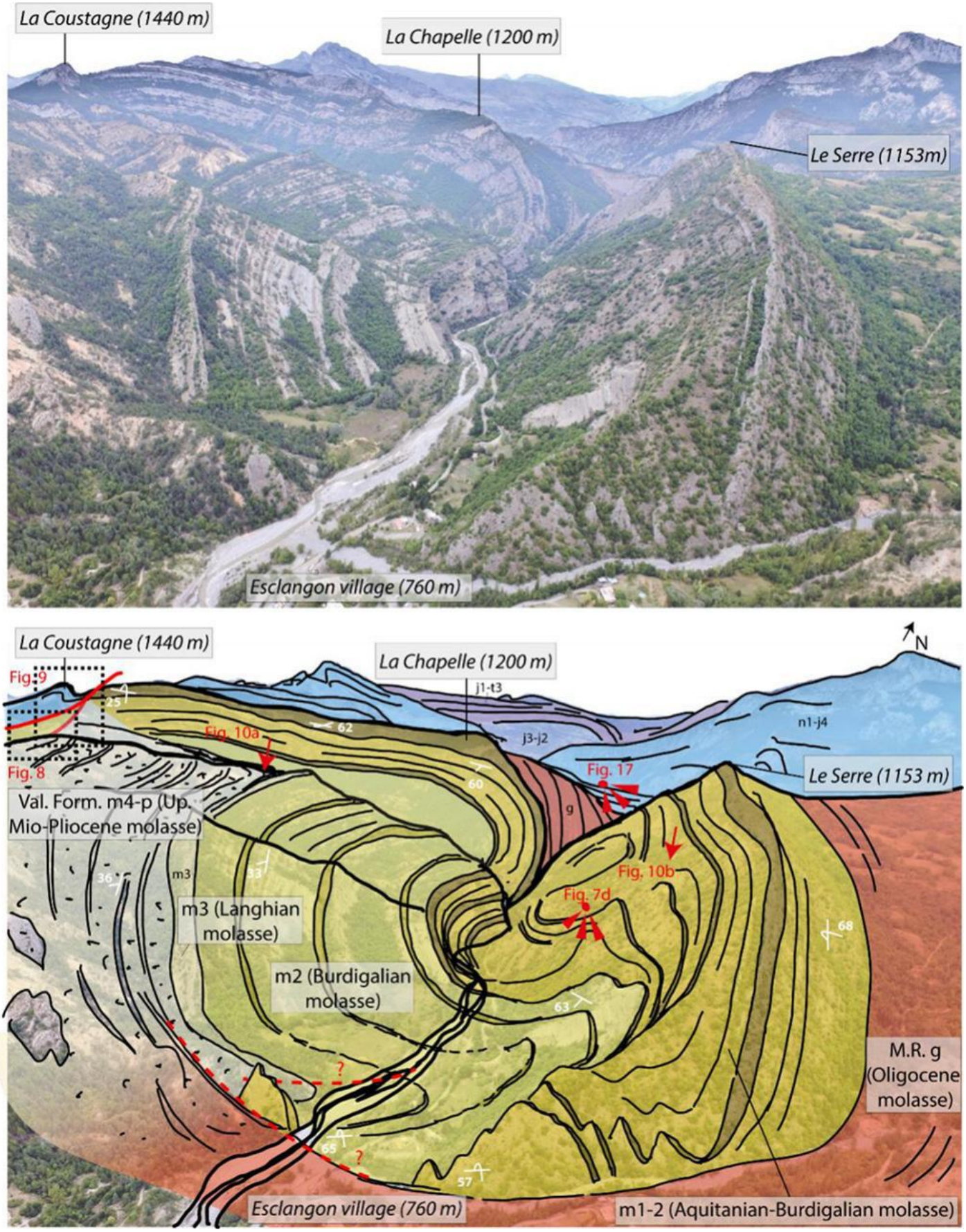
La Coustagne (1440 m)
La Chapelle (1200 m)
Le Serre (1153m)
Esclangon village (760 m)
La Coustagne (1440 m)
La Chapelle (1200 m)
N
Fig. 9
Fig. 8
Fig. 10a
Fig. 17
Fig. 10b
Fig. 7d
j1-t3
j3-j2
n1-j4
Le Serre (1153 m)
Val. Form. m4-p (Up. Mio-Pliocene molasse)
m3
m3 (Langhian molasse)
m2 (Burdigalian molasse)
g
M.R. g (Oligocene molasse)
m1-2 (Aquitanian-Burdigalian molasse)
Esclangon village (760 m)
25
62
60
36
33
68
63
65
57
?

Figure 3

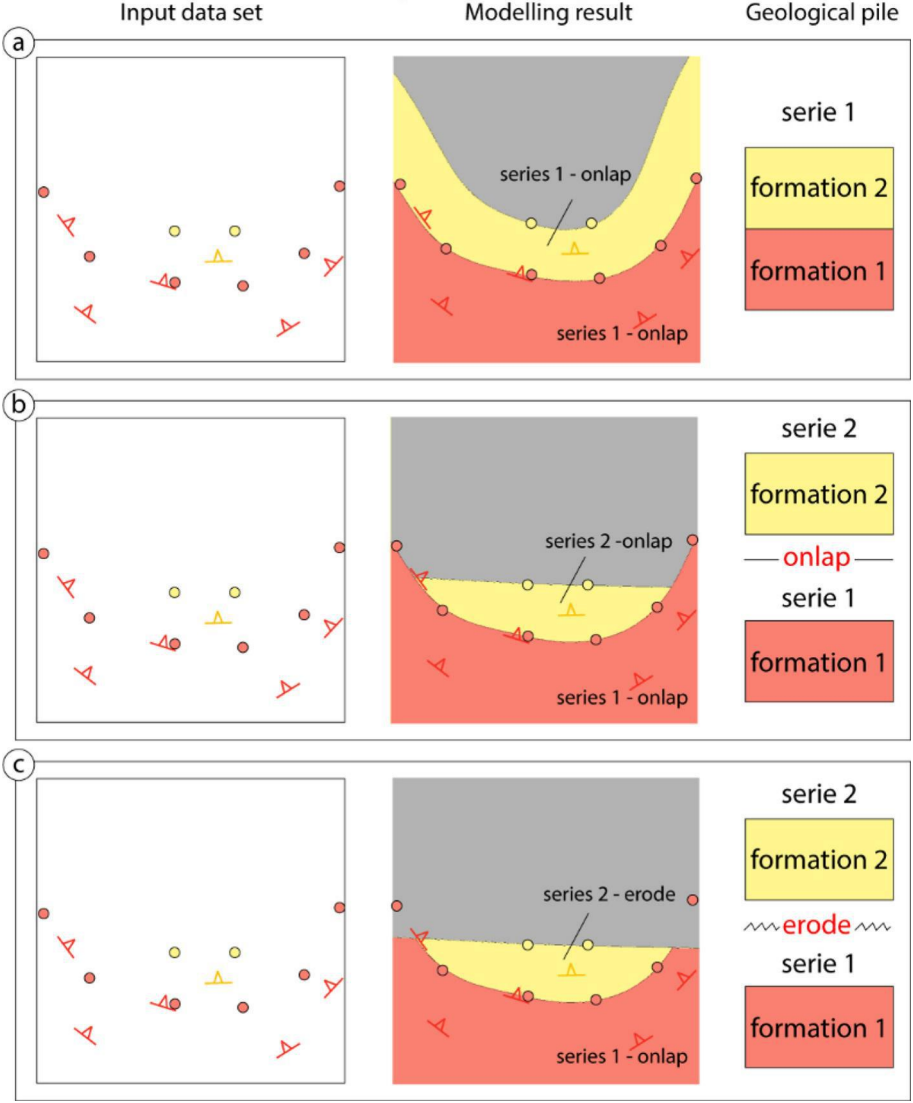
Input data set
Modelling result
Geological pile
a
series 1 - onlap
series 1 - onlap
serie 1
formation 2
formation 1
b
series 2 -onlap
series 1 - onlap
serie 2
formation 2
onlap
serie 1
formation 1
c
series 2 - erode
series 1 - onlap
serie 2
formation 2
erode
serie 1
formation 1

Figure 4

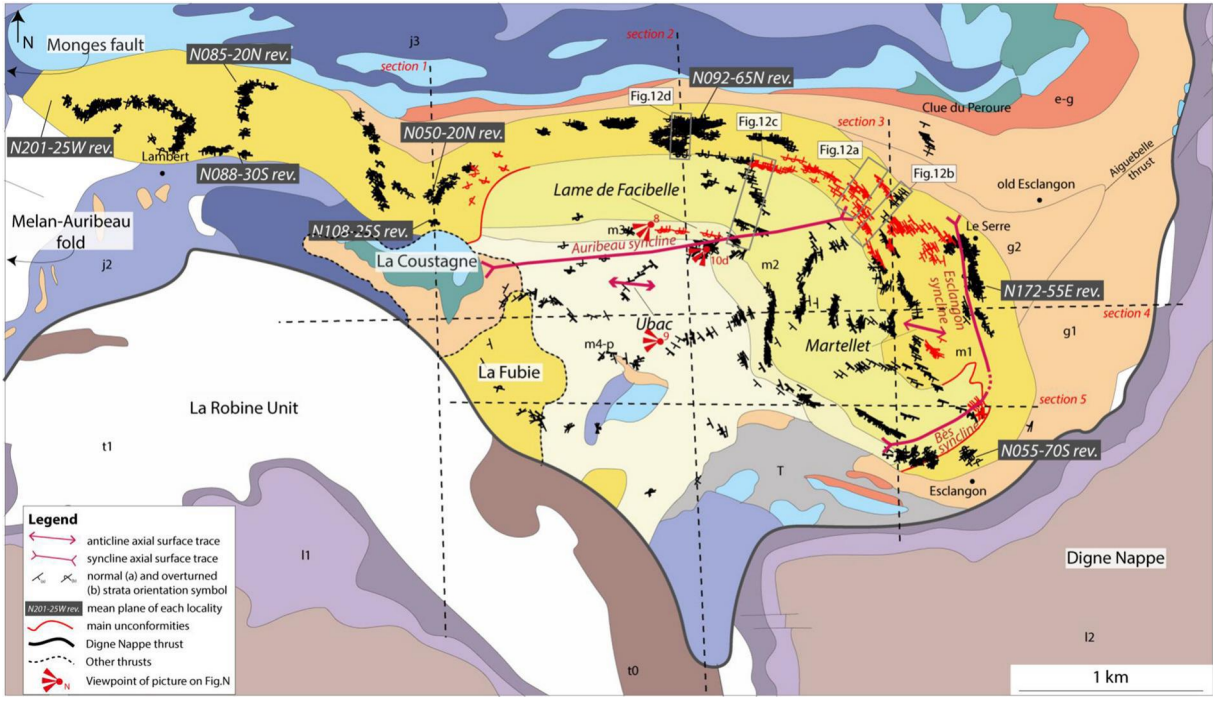
N
Monges fault
N085-20N rev.
N201-25W rev.
Lambert
N088-30S rev.
Melan-Auribeau fold
j2
j3
section 1
section 2
N092-65N rev.
Fig.12d
Fig.12c
Fig.12a
Fig.12b
section 3
Clue du Peroure
e-g
N050-20N rev.
Lame de Facibelle
old Esclangon
Aiguebelle thrust
Le Serre
g2
N108-25S rev.
La Coustagne
m3
Auribeau syncline
m2
Esclangon syncline
N172-55E rev.
section 4
g1
Ubac
m4-p
La Fubie
Martellet
m1
La Robine Unit
t1
section 5
Bès syncline
N055-70S rev.
T
Esclangon
Digne Nappe
l1
l2
t0
Legend
anticline axial surface trace
syncline axial surface trace
normal (a) and overturned (b) strata orientation symbol
N201-25W rev. mean plane of each locality
main unconformities
Digne Nappe thrust
Other thrusts
Viewpoint of picture on Fig.N
1 km

Figure 5

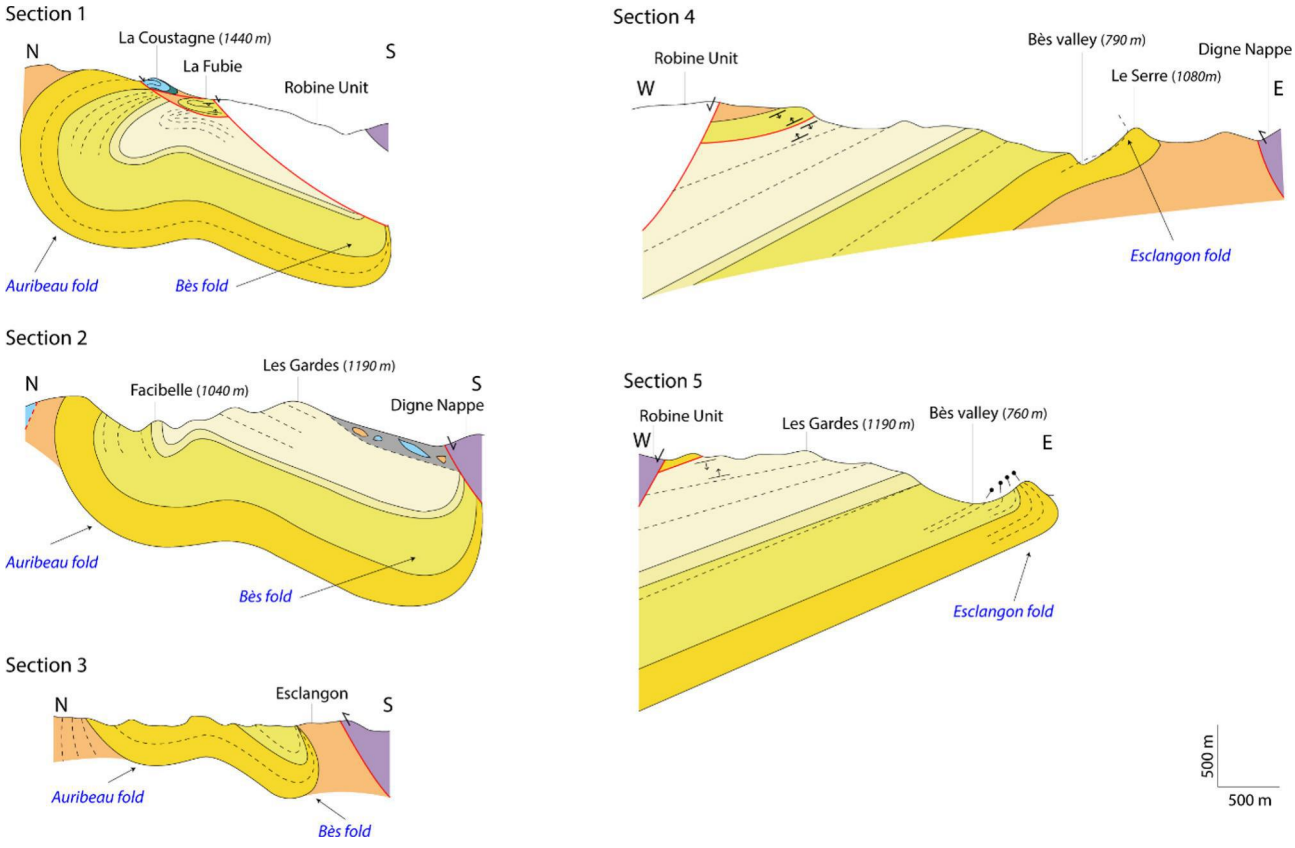
Section 1
N
La Coustagne (1440 m)
La Fubie
Robine Unit
S
Auribeau fold
Bès fold
Section 2
N
Facibelle (1040 m)
Les Gardes (1190 m)
S
Digne Nappe
Auribeau fold
Bès fold
Section 3
N
Esclangon
S
Auribeau fold
Bès fold
Section 4
Robine Unit
W
Bès valley (790 m)
Le Serre (1080m)
Digne Nappe
E
Esclangon fold
Section 5
Robine Unit
W
Les Gardes (1190 m)
Bès valley (760 m)
E
Esclangon fold
500 m
500 m

Figure 6

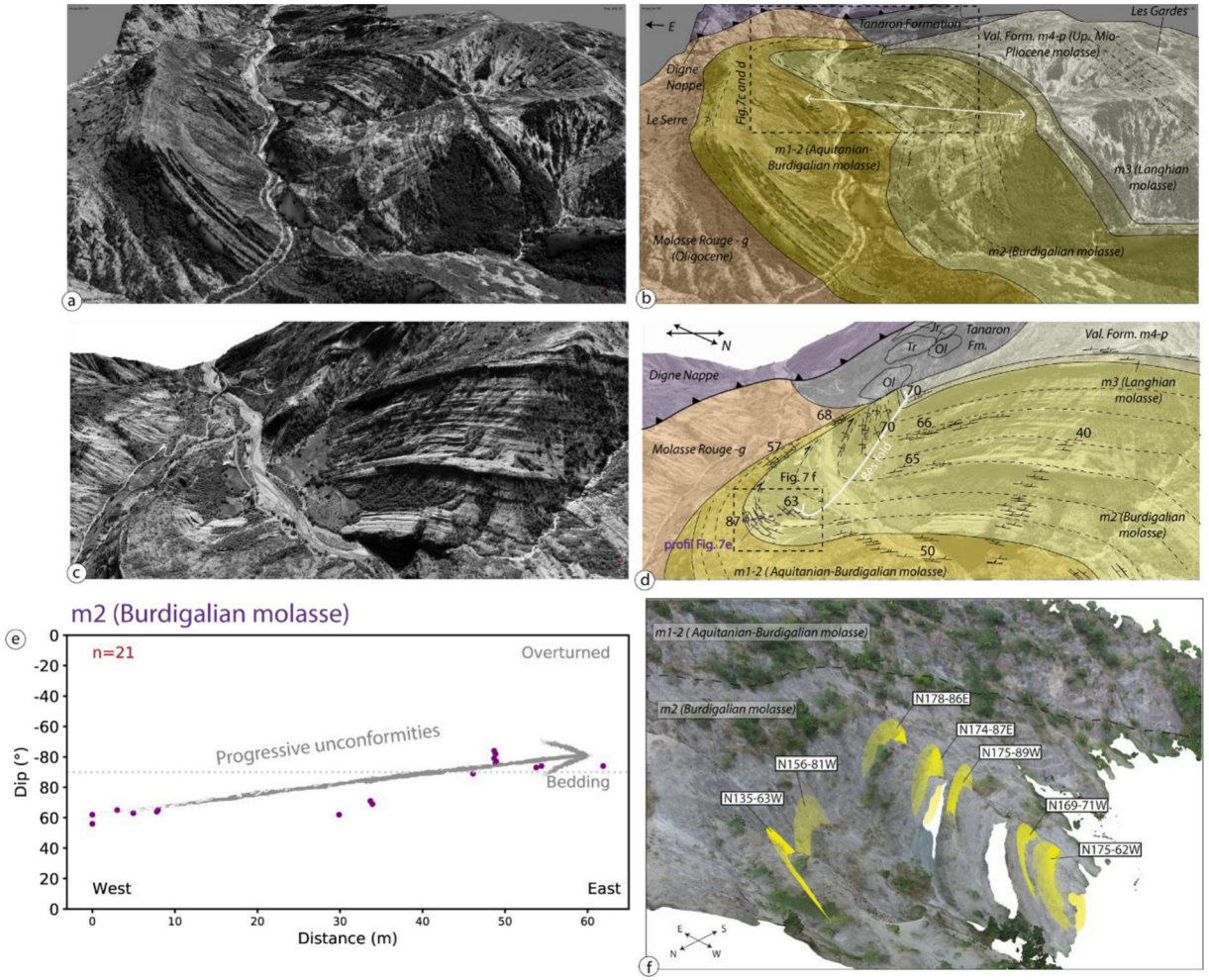
a
b
E
Tanaron Formation
Les Gardes
Val. Form. m4-p (Up.-Mio-Pliocene molasse)
Digne Nappe
Le Serre
Fig. 7 cond d
m1-2 (Aquitanian-Burdigalian molasse)
m3 (Langhian molasse)
Molasse Rouge - g (Oligocene)
m2 (Burdigalian molasse)
c
d
N
Tr.
Jr.
Ol
Tanaron Fm.
Val. Form. m4-p
Digne Nappe
m3 (Langhian molasse)
70
68
66
40
Molasse Rouge -g
57
65
Fig. 7 f
63
87
profil Fig. 7e
50
m2 (Burdigalian molasse)
m1-2 (Aquitanian-Burdigalian molasse)
e
m2 (Burdigalian molasse)
n=21
Overturned
Progressive unconformities
Bedding
Dip (°)
West
East
Distance (m)
f
m1-2 (Aquitanian-Burdigalian molasse)
m2 (Burdigalian molasse)
N178-86E
N174-87E
N175-89W
N156-81W
N135-63W
N169-71W
N175-62W

Figure 7

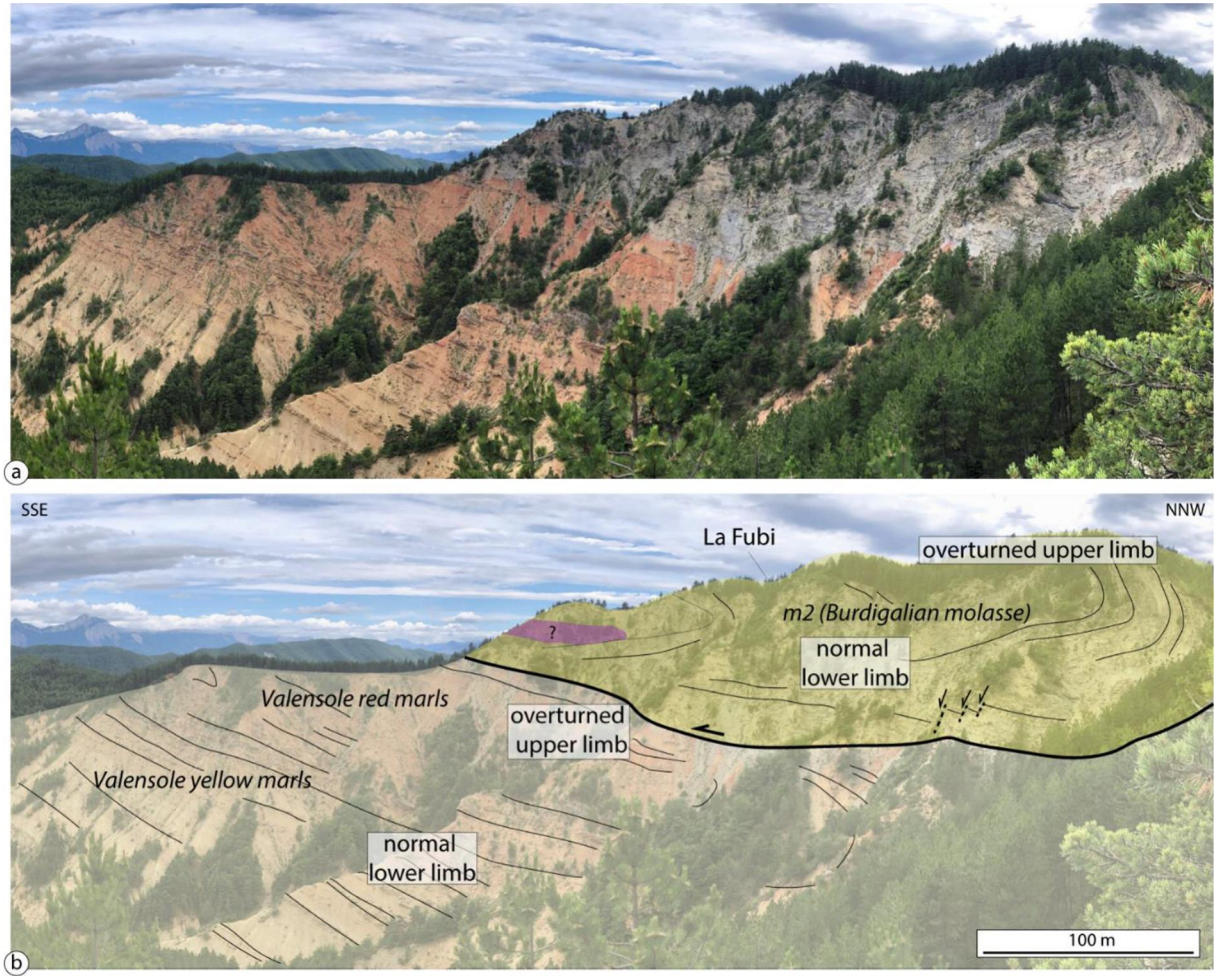
a
SSE
NNW
La Fubi
overturned upper limb
m2 (Burdigalian molasse)
?
normal
lower limb
Valensole red marls
overturned
upper limb
Valensole yellow marls
normal
lower limb
100 m
b

Figure 8

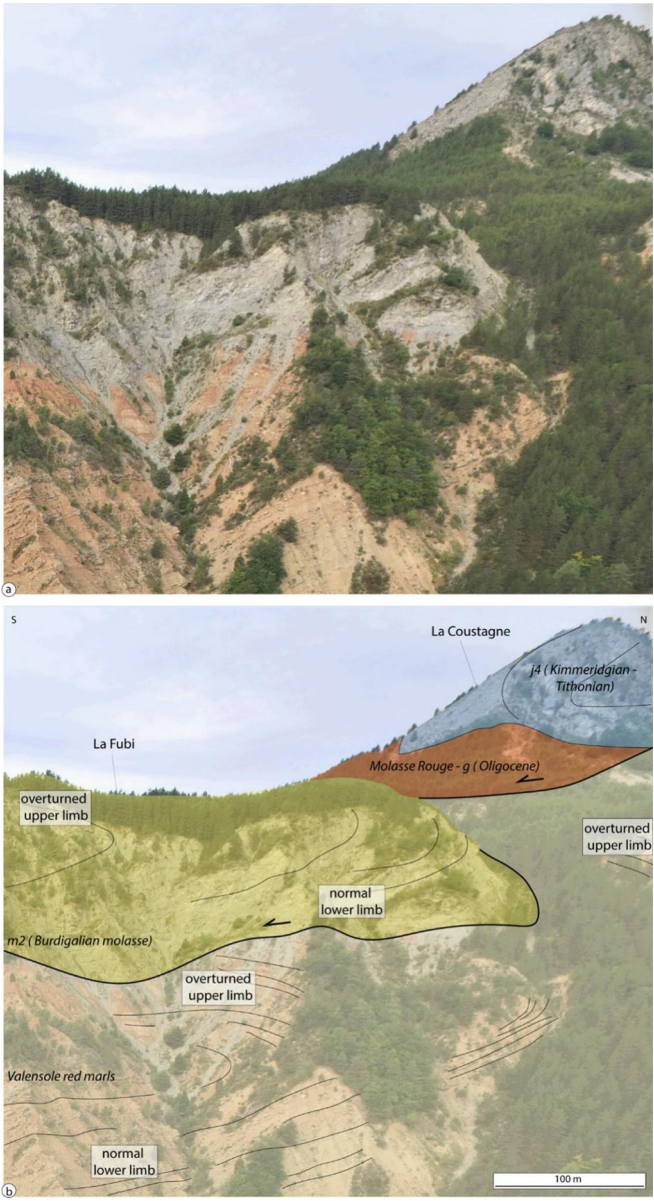
a
S
N
La Coustagne
j4 (Kimmeridgian - Tithonian)
La Fubi
Molasse Rouge - g (Oligocene)
overturned upper limb
overturned upper limb
normal lower limb
m2 (Burdigalian molasse)
overturned upper limb
Valensole red marls
normal lower limb
100 m
b

Figure 9

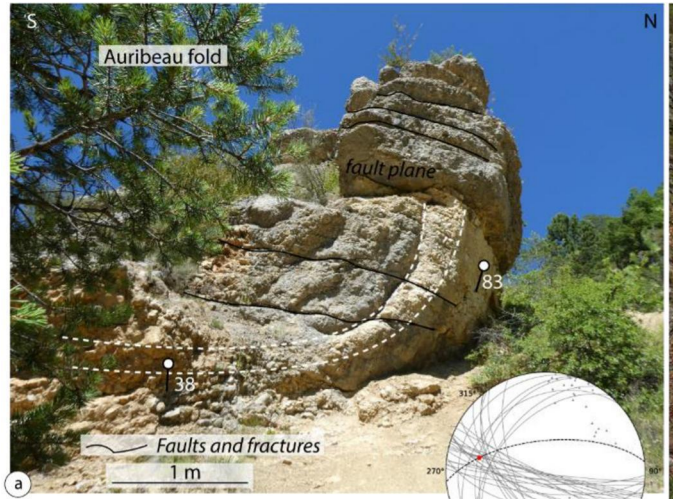

number of measure	fold	axial surface orientation	fold axis orientation
32	Auribeau	N084-64N	N282-33W

c

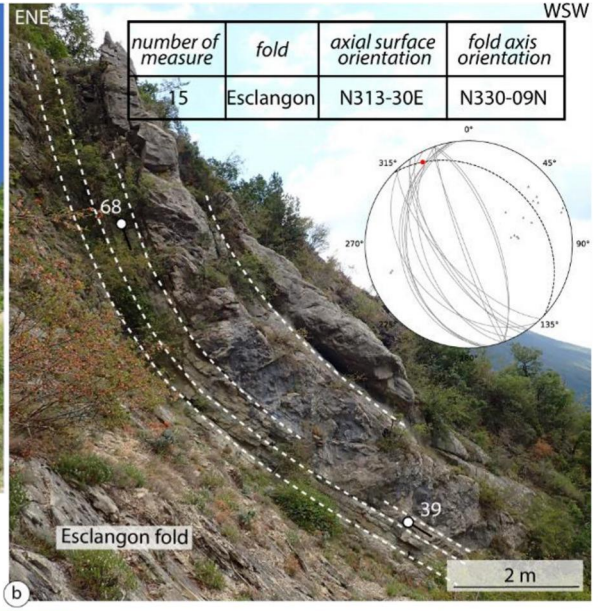

number of measure	fold	axial surface orientation	fold axis orientation
15	Esclangon	N313-30E	N330-09N

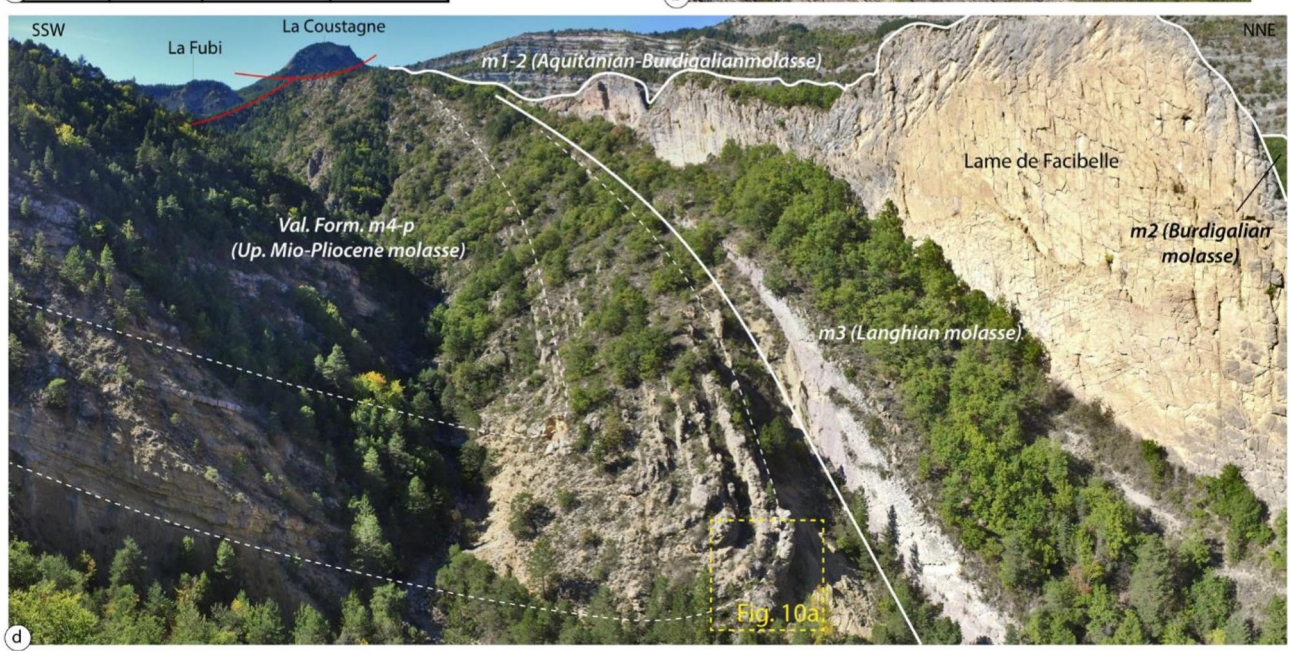

Figure 10

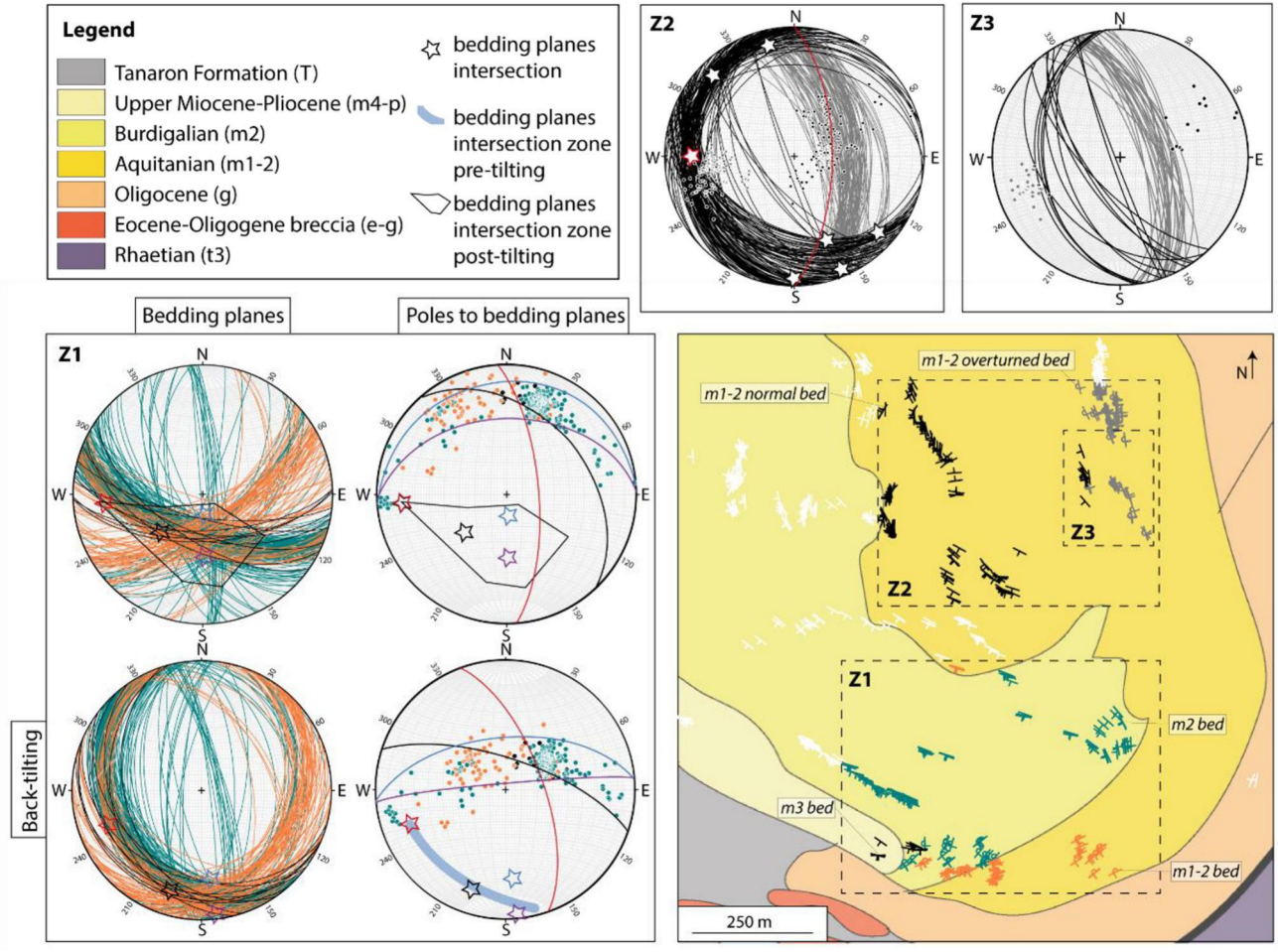
Legend
Tanaron Formation (T)
Upper Miocene-Pliocene (m4-p)
Burdigalian (m2)
Aquitanian (m1-2)
Oligocene (g)
Eocene-Oligogene breccia (e-g)
Rhaetian (t3)
bedding planes intersection
bedding planes intersection zone pre-tilting
bedding planes intersection zone post-tilting
Z2
Z3
Bedding planes
Poles to bedding planes
Z1
Back-tilting
m1-2 overturned bed
m1-2 normal bed
Z3
Z2
Z1
m2 bed
m3 bed
m1-2 bed
250 m

Figure 11

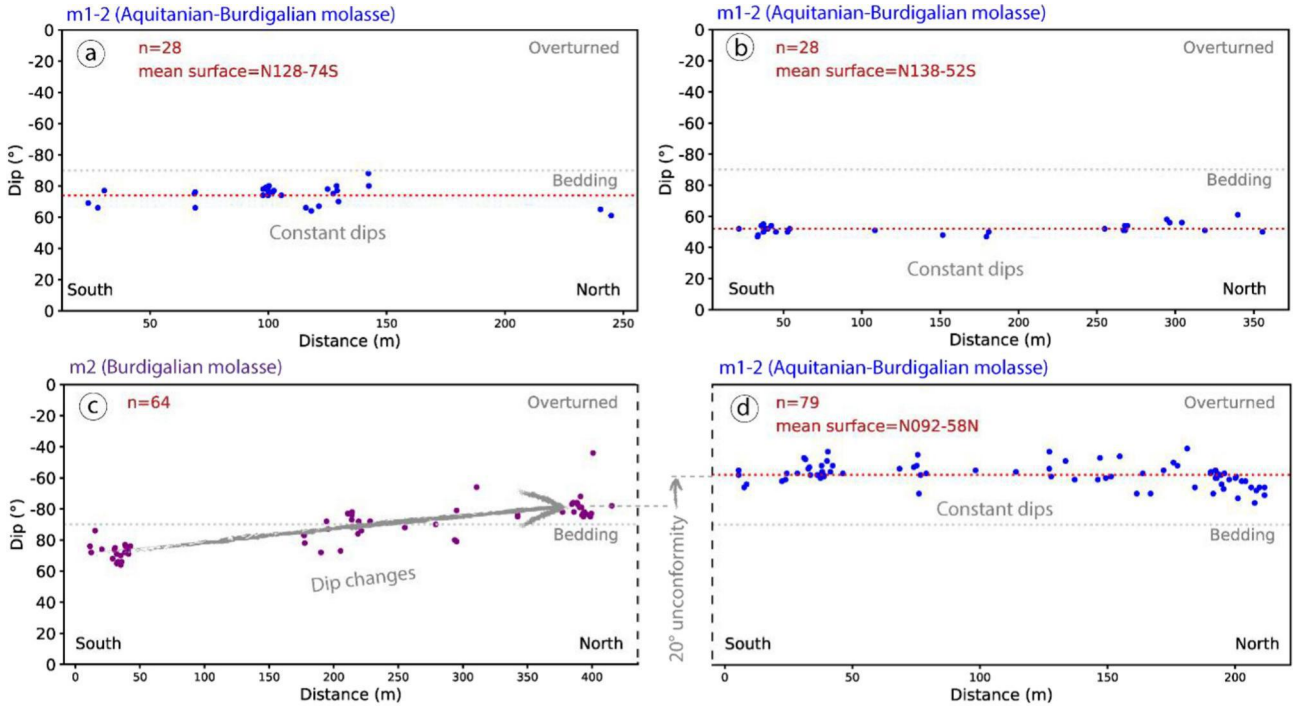

*a lateral distance of 500 m separates the end of the profile c) from the beginning of the profile d)

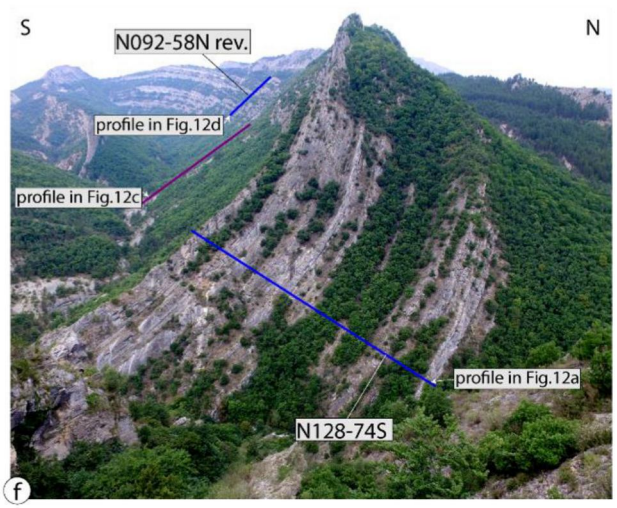

Figure 12

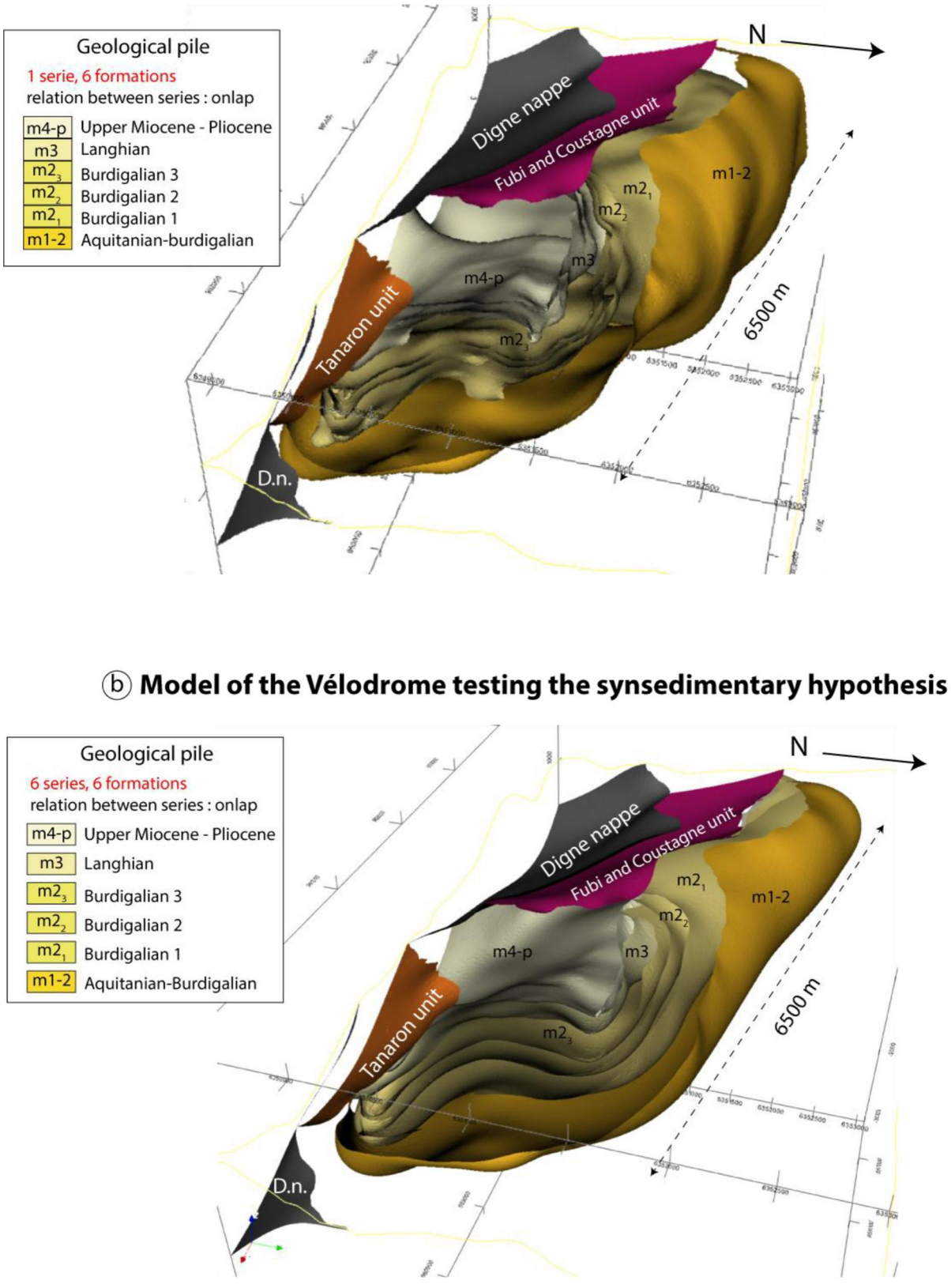
a Model of the Vélodrome testing the postsedimentary hypothesis
Geological pile
1 serie, 6 formations
relation between series : onlap
m4-p Upper Miocene - Pliocene
m3 Langhian
m2$_3$ Burdigalian 3
m2$_2$ Burdigalian 2
m2$_1$ Burdigalian 1
m1-2 Aquitanian-burdigalian
N
Digne nappe
Fubi and Coustagne unit
m1-2
m2$_1$
m2$_2$
m3
m4-p
m2$_3$
Tanaron unit
6500 m
D.n.
b Model of the Vélodrome testing the synsedimentary hypothesis
Geological pile
6 series, 6 formations
relation between series : onlap
m4-p Upper Miocene - Pliocene
m3 Langhian
m2$_3$ Burdigalian 3
m2$_2$ Burdigalian 2
m2$_1$ Burdigalian 1
m1-2 Aquitanian-Burdigalian
N
Digne nappe
Fubi and Coustagne unit
m2$_1$
m1-2
m2$_2$
m4-p
m3
m2$_3$
Tanaron unit
6500 m
D.n.

Figure 13

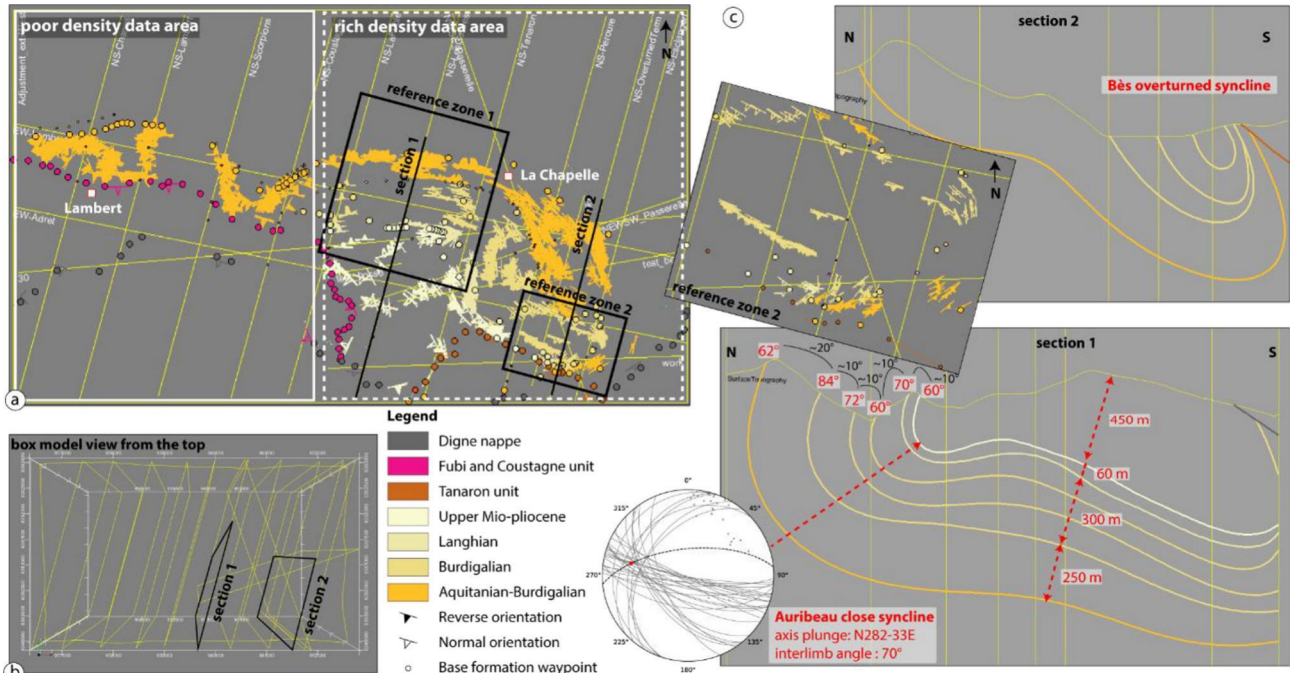
poor density data area
rich density data area
reference zone 1
section 1
La Chapelle
section 2
reference zone 2
Lambert
N
a
c
section 2
N
S
Bès overturned syncline
reference zone 2
section 1
62°
84°
72°
60°
70°
60°
~20°
~10°
~10°
~10°
~10°
450 m
60 m
300 m
250 m
Auribeau close syncline
axis plunge: N282-33E
interlimb angle : 70°
box model view from the top
section 1
section 2
b
Legend
Digne nappe
Fubi and Coustagne unit
Tanaron unit
Upper Mio-pliocene
Langhian
Burdigalian
Aquitanian-Burdigalian
Reverse orientation
Normal orientation
Base formation waypoint

Figure 14

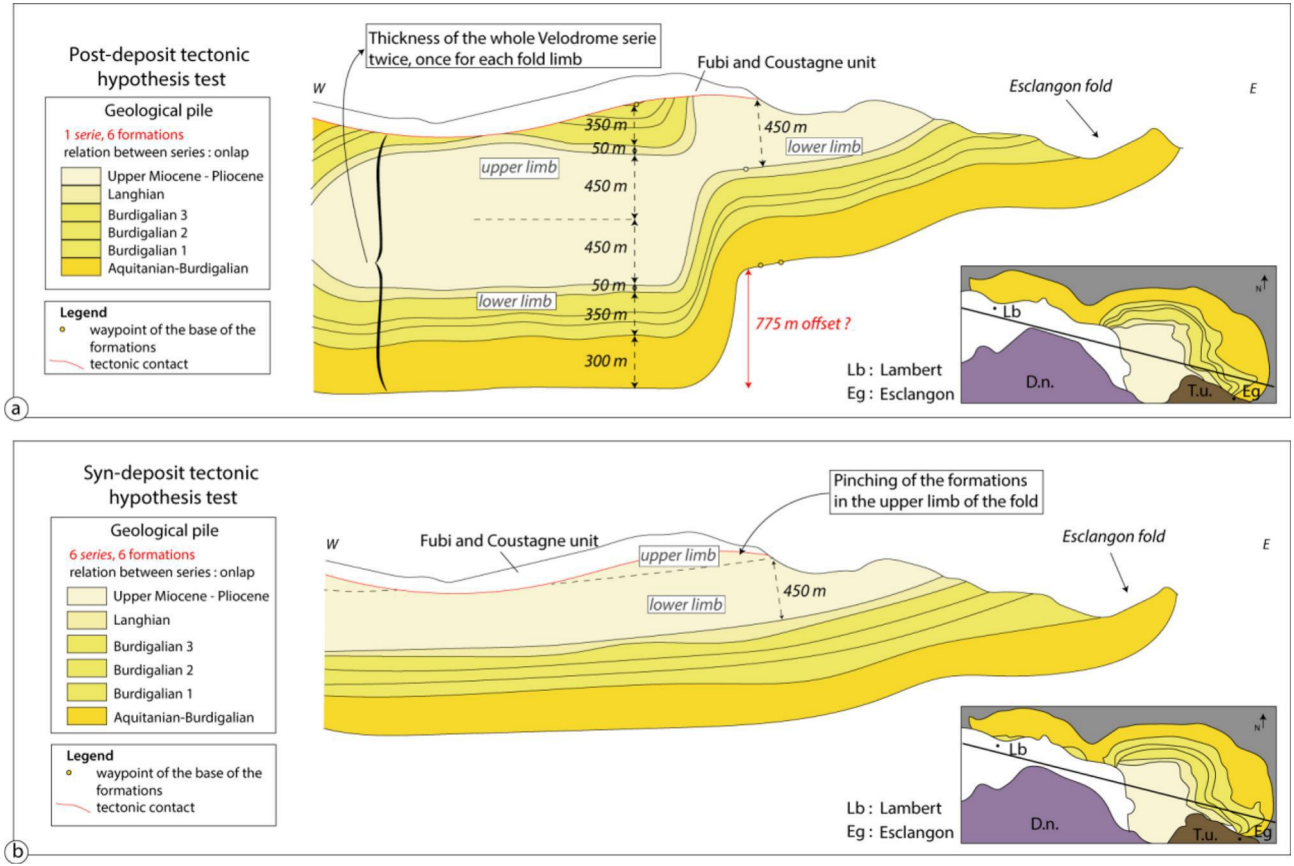
Post-deposit tectonic hypothesis test
Geological pile
1 serie, 6 formations
relation between series : onlap
Upper Miocene - Pliocene
Langhian
Burdigalian 3
Burdigalian 2
Burdigalian 1
Aquitanian-Burdigalian
Legend
waypoint of the base of the formations
tectonic contact
Thickness of the whole Velodrome serie twice, once for each fold limb
Fubi and Coustagne unit
Esclangon fold
W
E
350 m
50 m
450 m
upper limb
450 m
lower limb
450 m
50 m
lower limb
350 m
300 m
775 m offset ?
Lb
D.n.
T.u.
Eg
Lb : Lambert
Eg : Esclangon
a
Syn-deposit tectonic hypothesis test
Geological pile
6 series, 6 formations
relation between series : onlap
Upper Miocene - Pliocene
Langhian
Burdigalian 3
Burdigalian 2
Burdigalian 1
Aquitanian-Burdigalian
Legend
waypoint of the base of the formations
tectonic contact
Pinching of the formations in the upper limb of the fold
W
Fubi and Coustagne unit
upper limb
lower limb
450 m
Esclangon fold
E
Lb
D.n.
T.u.
Eg
Lb : Lambert
Eg : Esclangon
b

Figure 15

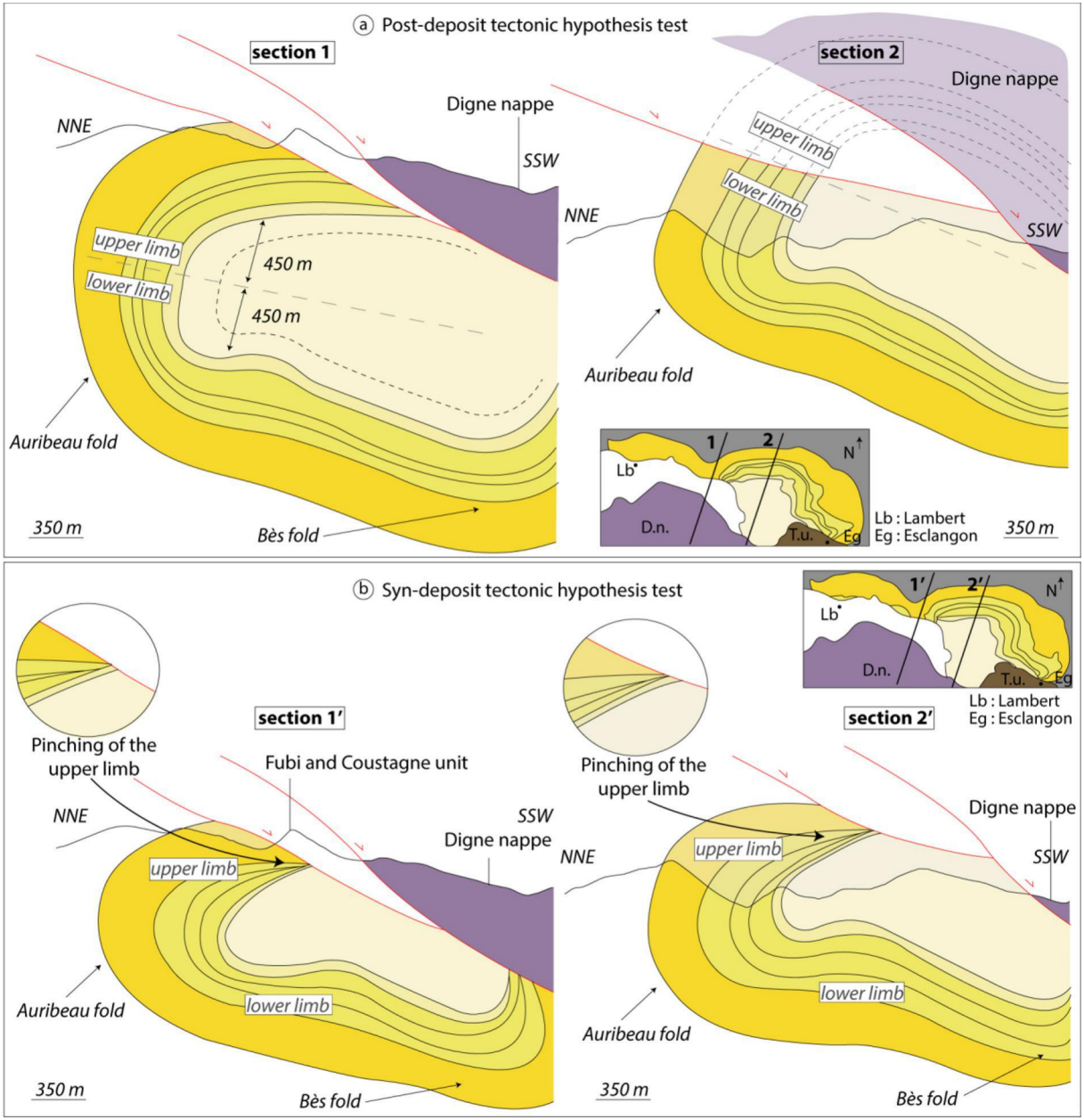
ⓐ Post-deposit tectonic hypothesis test
section 1
NNE
Digne nappe
SSW
upper limb
lower limb
450 m
450 m
Auribeau fold
350 m
Bès fold
section 2
Digne nappe
upper limb
lower limb
NNE
SSW
Auribeau fold
1
2
N
Lb
D.n.
T.u.
Eg
Lb : Lambert
Eg : Esclangon
350 m
ⓑ Syn-deposit tectonic hypothesis test
1′
2′
N
Lb
D.n.
T.u.
Eg
Lb : Lambert
Eg : Esclangon
Pinching of the upper limb
section 1′
Fubi and Coustagne unit
NNE
SSW
Digne nappe
upper limb
Auribeau fold
lower limb
350 m
Bès fold
Pinching of the upper limb
section 2′
Digne nappe
NNE
upper limb
SSW
lower limb
Auribeau fold
350 m
Bès fold

Figure 16

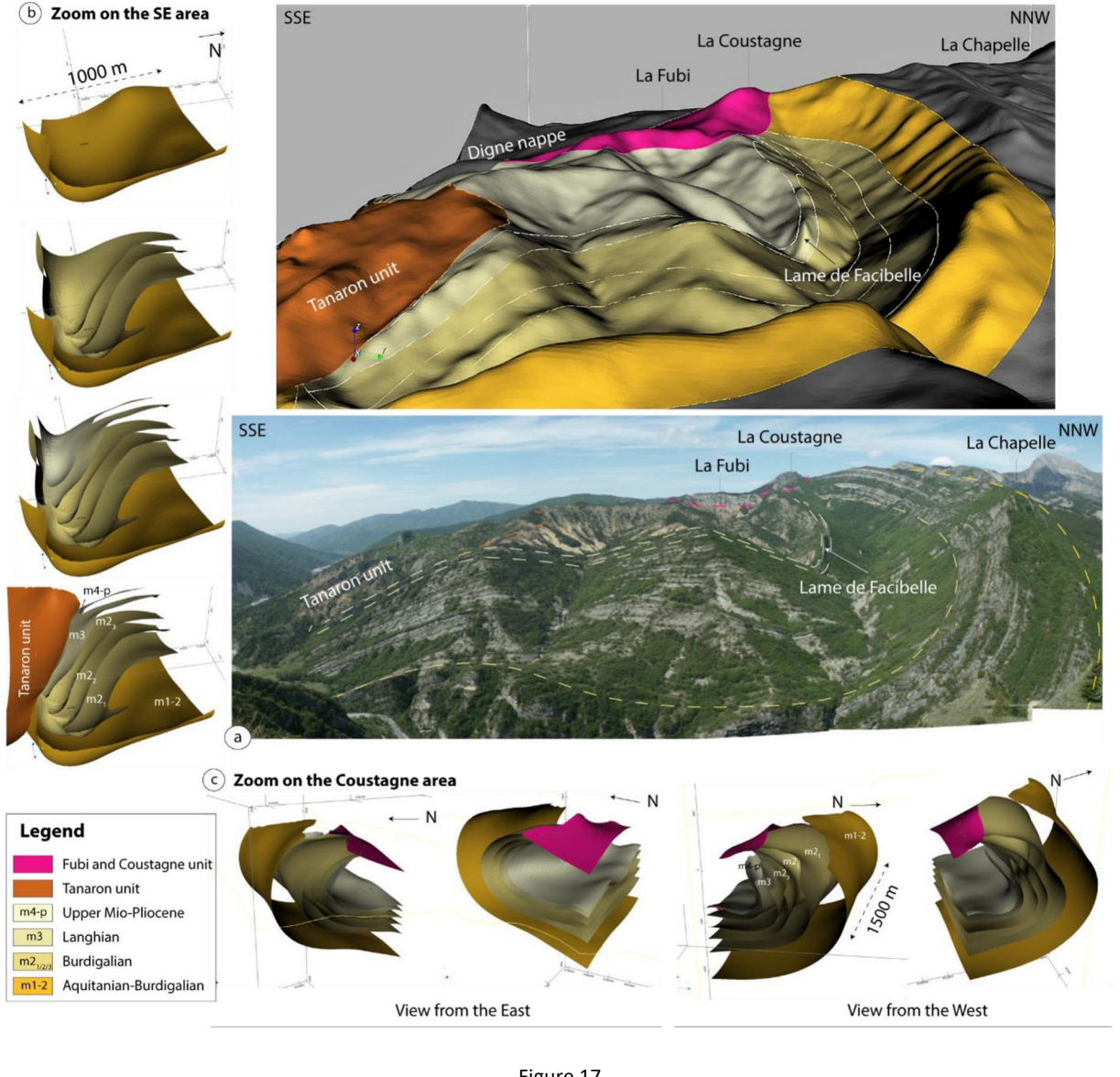
b Zoom on the SE area
1000 m
N
SSE
NNW
La Coustagne
La Chapelle
La Fubi
Digne nappe
Tanaron unit
Lame de Facibelle
SSE
NNW
La Coustagne
La Chapelle
La Fubi
Tanaron unit
Lame de Facibelle
a
m4-p
m2
m3
m2
m2
m1-2
Tanaron unit
c Zoom on the Coustagne area
N
N
N
N
m1-2
m2
m4-p
m2
m3
1500 m
Legend
Fubi and Coustagne unit
Tanaron unit
m4-p Upper Mio-Pliocene
m3 Langhian
m2 Burdigalian
m1-2 Aquitanian-Burdigalian
View from the East
View from the West

Figure 17

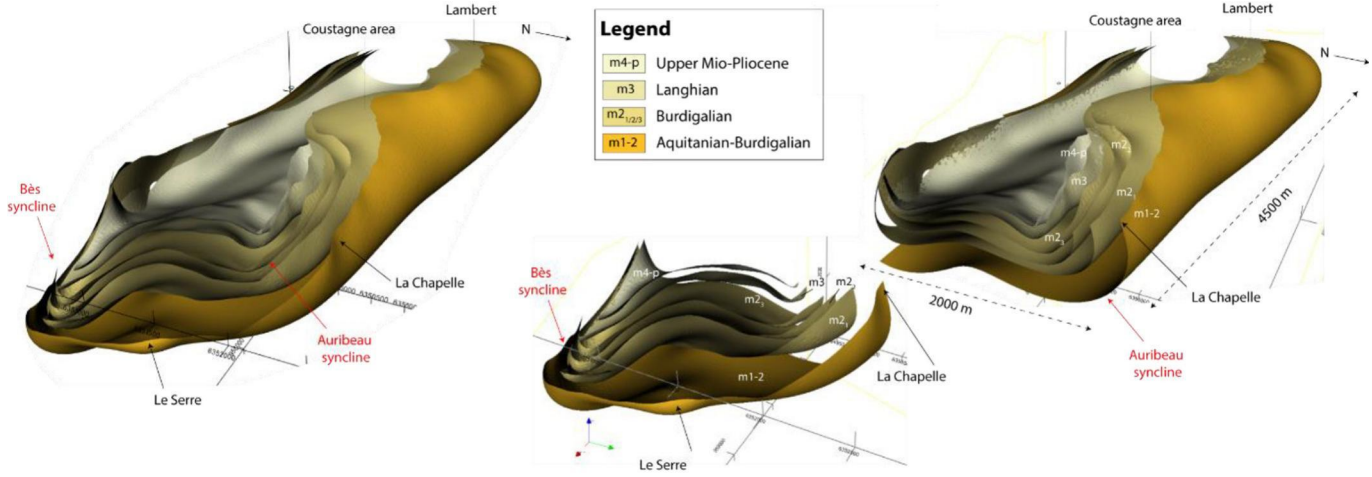

Formation bottom surfaces modelled

Formation bottom surfaces modelled clipped near La Chapelle

Figure 18

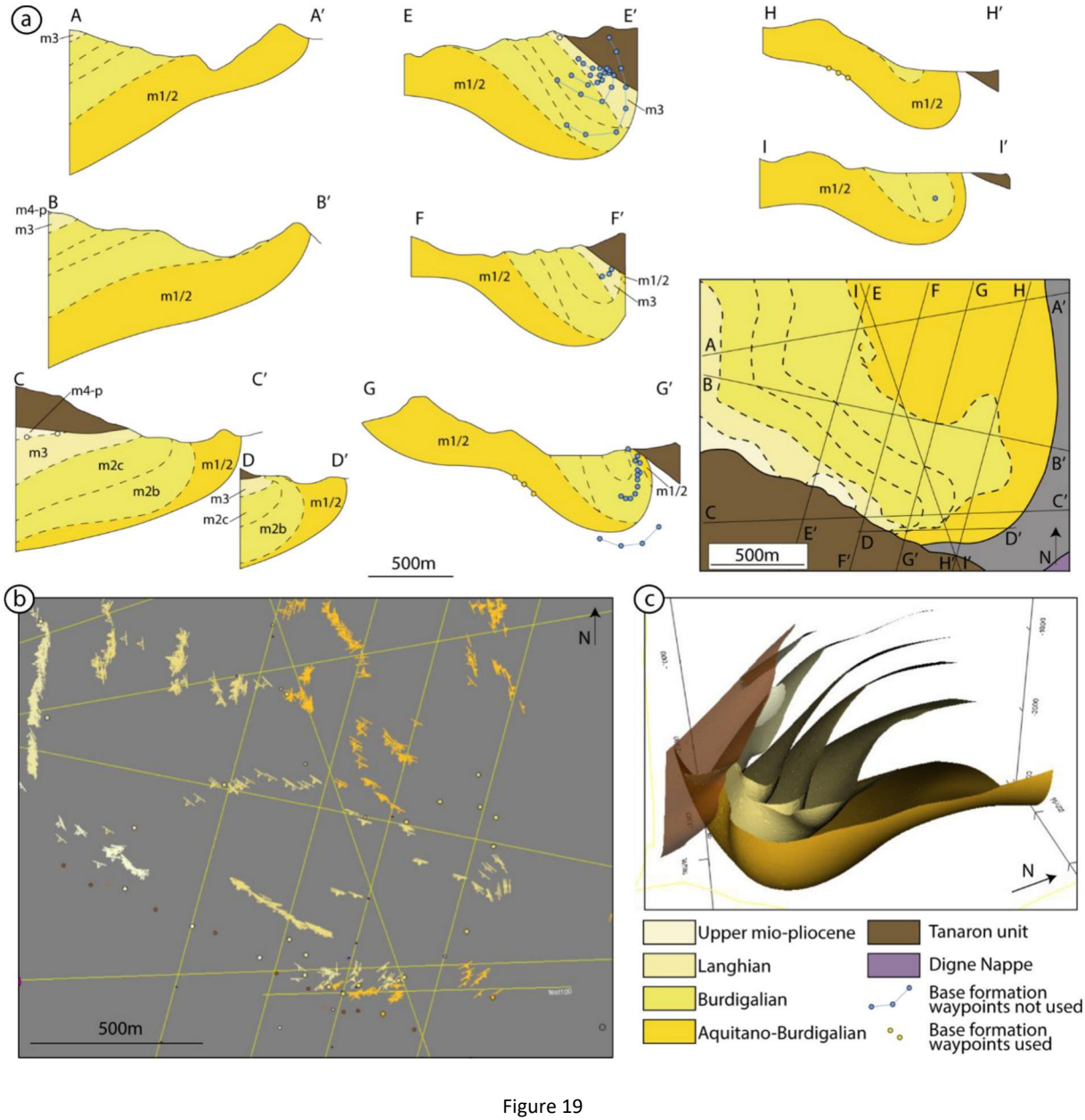
a
A
A′
m3
m1/2
E
E′
m1/2
m3
H
H′
m1/2
I
I′
m1/2
B
B′
m4-p
m3
m1/2
F
F′
m1/2
m1/2
m3
C
C′
m4-p
m3
m2c
m2b
m1/2
D
D′
m3
m2c
m2b
m1/2
G
G′
m1/2
m1/2
500m
I
E
F
G
H
A′
A
B
B′
C
C′
E′
D
D′
F′
G′
H′
I′
N
500m
b
N
500m
c
N
Upper mio-pliocene
Langhian
Burdigalian
Aquitano-Burdigalian
Tanaron unit
Digne Nappe
Base formation waypoints not used
Base formation waypoints used

Figure 19

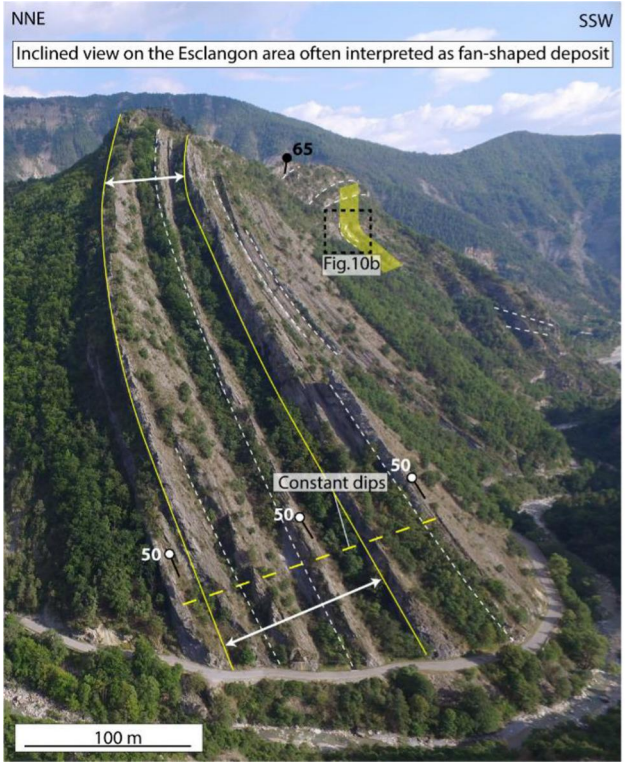
NNE
SSW
Inclined view on the Esclangon area often interpreted as fan-shaped deposit
65
Fig.10b
Constant dips
50
50
50
100 m

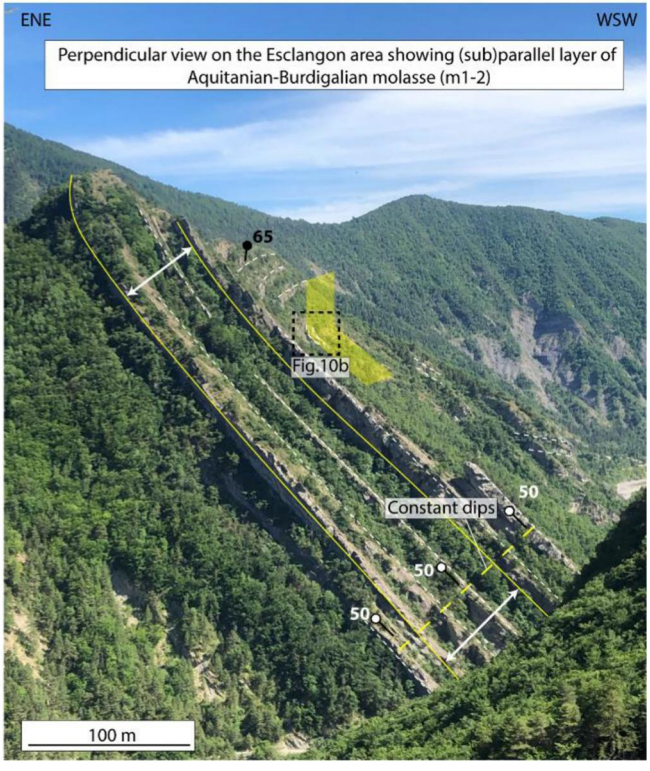
ENE
WSW
Perpendicular view on the Esclangon area showing (sub)parallel layer of Aquitanian-Burdigalian molasse (m1-2)
65
Fig.10b
Constant dips
50
50
50
100 m

Figure 20

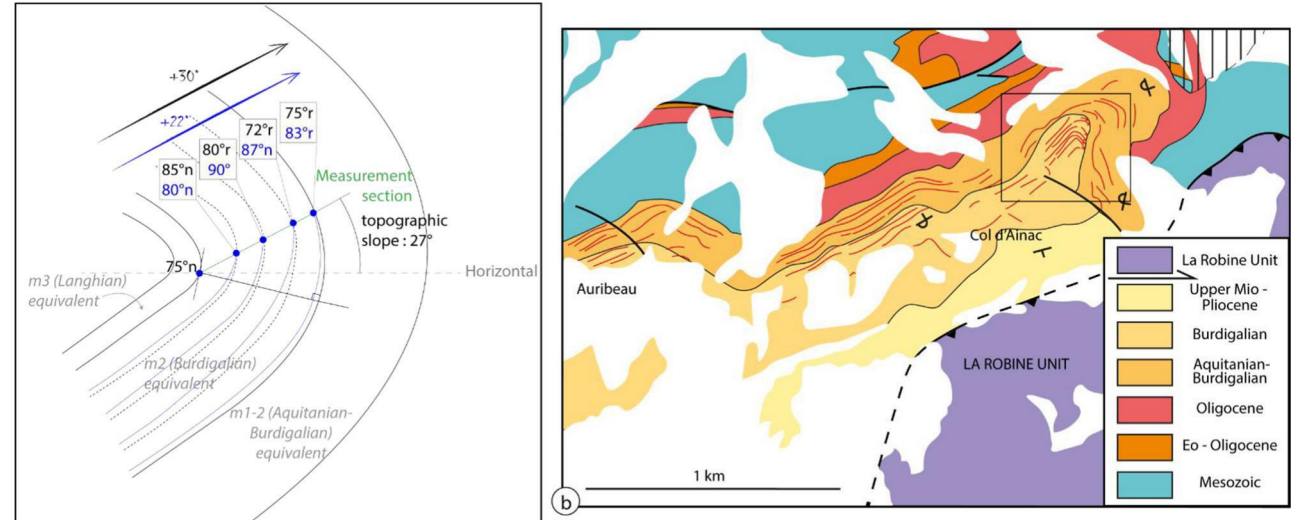
+30°
+22°
75°r
83°r
72°r
87°n
80°r
90°
85°n
80°n
Measurement
section
topographic
slope : 27°
75°n
Horizontal
m3 (Langhian)
equivalent
m2 (Burdigalian)
equivalent
m1-2 (Aquitanian-
Burdigalian)
equivalent
a
Col d'Ainac
Auribeau
LA ROBINE UNIT
1 km
b
La Robine Unit
Upper Mio -
Pliocene
Burdigalian
Aquitanian-
Burdigalian
Oligocene
Eo - Oligocene
Mesozoic

Figure 21

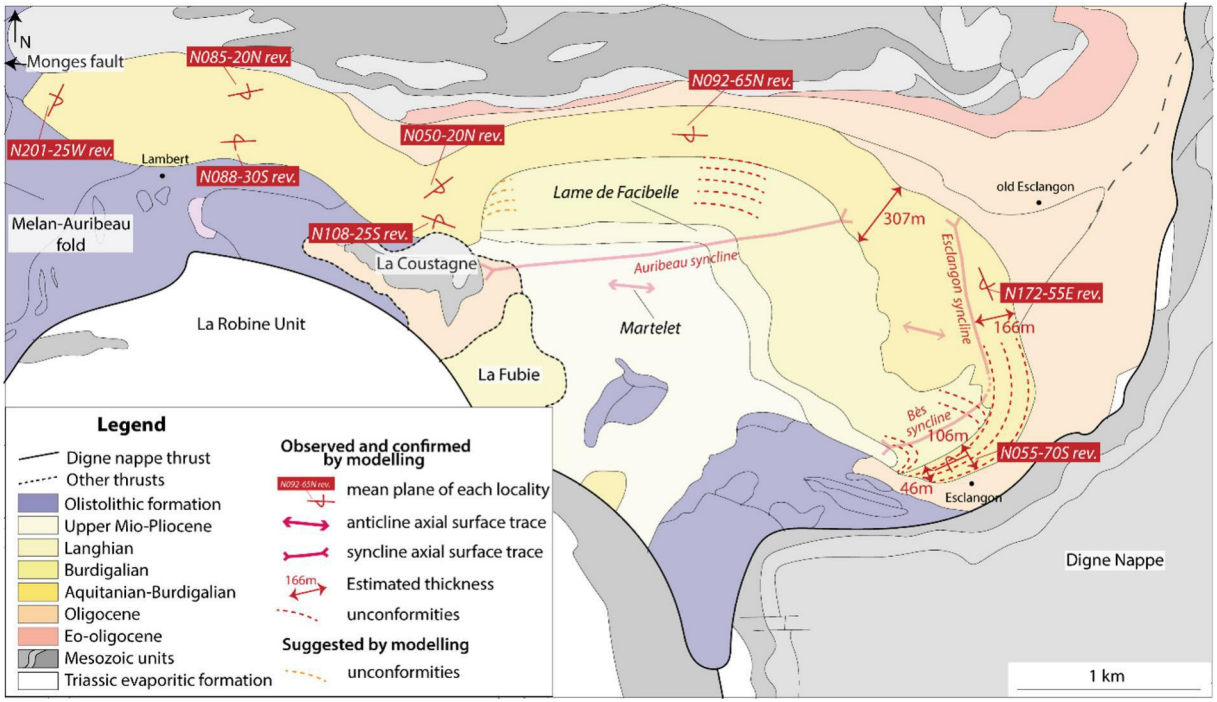
N
Monges fault
N085-20N rev.
N092-65N rev.
N050-20N rev.
N201-25W rev.
Lambert
N088-30S rev.
Lame de Facibelle
old Esclangon
Melan-Auribeau fold
N108-25S rev.
307m
La Coustagne
Auribeau syncline
Esclangon syncline
N172-55E rev.
La Robine Unit
Martelet
166m
La Fubie
Bès syncline
106m
N055-70S rev.
46m
Esclangon
Digne Nappe
1 km
Legend
Digne nappe thrust
Other thrusts
Olistolithic formation
Upper Mio-Pliocene
Langhian
Burdigalian
Aquitanian-Burdigalian
Oligocene
Eo-oligocene
Mesozoic units
Triassic evaporitic formation
Observed and confirmed by modelling
N092-65N rev.
mean plane of each locality
anticline axial surface trace
syncline axial surface trace
166m
Estimated thickness
unconformities
Suggested by modelling
unconformities

Figure 22

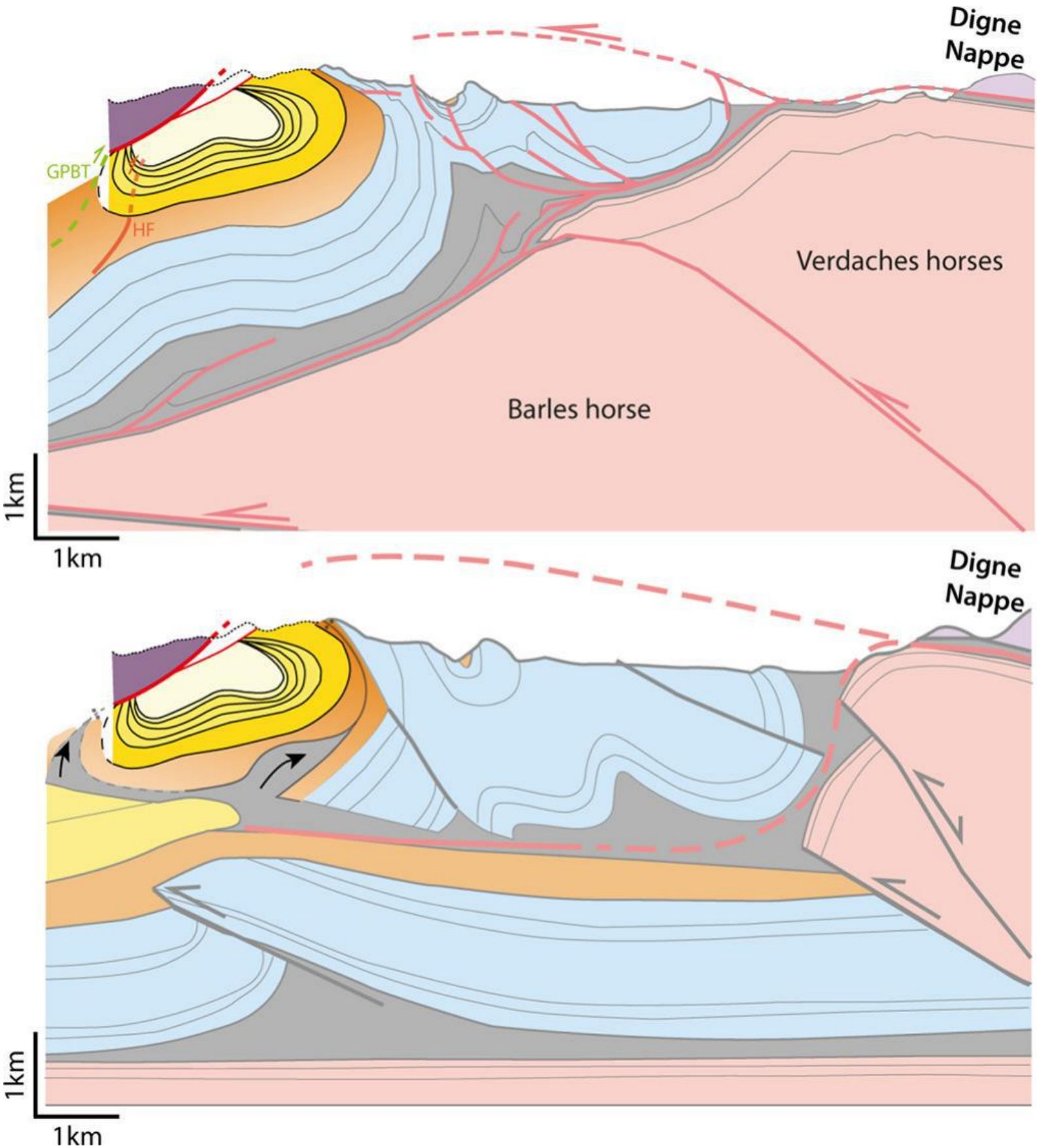
Digne
Nappe
GPBT
HF
Verdaches horses
Barles horse
1km
1km
Digne
Nappe
1km
1km

Figure 23